https://doi.org/10.5194/acp-2020-864
Preprint. Discussion started: 31 August 2020

Atmospheric Chemistry and Physics Discussions

On the relationship between tropospheric CO and CO_2 during KORUS-AQ and its role in constraining anthropogenic CO_2

Wenfu Tang[1,2*], Benjamin Gaubert[2], Louisa Emmons[2], Yonghoon Choi[3,4], Joshua P. DiGangi[3], Glenn S. Diskin[3], Xiaomei Xu[5], Cenlin He[6], Helen Worden[2], Simone Tilmes[2], Rebecca Buchholz[2], Hannah S. Halliday[3,7] and Avelino F. Arellano[1]

[1]Department of Hydrology and Atmospheric Sciences, University of Arizona, Tucson, AZ, USA

[2]Atmospheric Chemistry Observations and Modeling Laboratory, National Center for Atmospheric Research, Boulder, CO, USA

[3]NASA Langley Research Center, Hampton, VA, USA

[4]Science Systems and Applications, Inc., Hampton, VA, USA

[5]Department of Earth System Science, University of California, Irvine, CA, USA

[6]Research Applications Laboratory, National Center for Atmospheric Research, Boulder, CO, USA

[7]Now at US Environmental Protection Agency, Research Triangle Park, Durham, NC, USA

Corresponding author: Avelino Arellano (afarellano@email.arizona.edu)

https://doi.org/10.5194/acp-2020-864
Preprint. Discussion started: 31 August 2020

Atmospheric Chemistry and Physics Discussions

Abstract

While the complementarity of CO data in monitoring CO_2 from fossil-fuel combustion ($ffCO_2$) is widely known, a rigorous demonstration of its use in reducing uncertainties on top-down regional $ffCO_2$ emissions is still warranted. Here, we report a case study investigating the regional covariation of observed and modeled abundances of CO, CO_2, and $ffCO_2$ and demonstrating its implication to joint CO:CO_2 inversions. We use data from a recent aircraft field campaign (KORUS-AQ) conducted over Korea and neighboring regions on May 2016 for this case study. We use the Community Atmosphere Model with Chemistry (CAM-Chem) to simulate CO, CO_2, $ffCO_2$ and associated source tags, using *a posteriori* fluxes from global CO_2 flux inversions and CO emissions independently calibrated against CO data. Among other model-data comparisons, CAM-Chem simulations show an underestimation in CO_2 (1 ppm), CO (24 ppb) and $ffCO_2$ (1 ppm) against aircraft measurements. These are all within the range of model and data uncertainties. Although the overall observed enhancement ratio, $\Delta CO/\Delta CO_2$ (~13.3±0.21 ppb/ppm), is well captured by CAM-Chem (~13.8±0.23 ppb/ppm), we find an overestimation (29 ppb/ppm) for air samples between 2 to 3 km, where East Asian influence is substantial (35%). The contribution of $ffCO_2$ from Korea and Japan is smaller (30%) and localized below 3 km, suggesting that regional $ffCO_2$ and background and non-$ffCO_2$ cannot be neglected in interpreting observed enhancements in this region. These spatial variations translate in the joint CO:CO_2 inversion to increases in *a posteriori* $ffCO_2$ estimates from East Asia (27%±24%) and Korea and Japan (9%±17%). This is consistent (albeit larger in 1-sigma uncertainty) with our estimate using $^{14}CO_2$ data (27%±9% and 10%±3%, respectively). In contrast, the inversion using only CO_2 data shows a decrease by ~5%±27% in East Asia and ~6%±19% in Korea and Japan. Our results show that inversions using both CO_2 and CO can be an effective approach in constraining $ffCO_2$ when the regional variations of CO and CO_2 relationships are appropriately accounted for. Although this further points to the potential of augmenting current observing system of CO_2 with CO for global inverse analyses of $ffCO_2$ from different regions of the globe, we highlight the need to verify the spatiotemporal distribution of the covariation of CO with CO_2 in both regional and global models. We caution its use for constraining local $ffCO_2$, unless the spatiotemporal *a priori* flux distribution and surface processes are reasonably represented, as they may confound the analysis. These have important implications on inversion studies using columnar data from satellite observations, especially for regions lacking necessary verification measurements.

https://doi.org/10.5194/acp-2020-864
Preprint. Discussion started: 31 August 2020


Atmospheric Chemistry and Physics Discussions

1. Introduction

Reducing the uncertainty on top-down estimates of carbon dioxide emissions from fossil fuel combustion ($ffCO_2$) continues to be a challenge. This is due to the dearth of accurate CO_2 measurements, including $^{14}CO_2$-derived $ffCO_2$ measurements, with sufficient spatiotemporal coverage necessary to resolve variations in combustion and fuel-use patterns, along with difficulty in teasing out small anthropogenic signature from the large natural sources and sinks dominating the carbon cycle, and the uncertainties in modeling atmospheric transport (e.g., NRC, 2010; Ciais et al. 2014). This challenge remains despite the addition of aircraft and satellite measurements of CO_2 abundance in recent years (e.g., Hungershoefer et al. 2010; Chevallier et al., 2014; Houweling et al., 2015). Understandably, global atmospheric CO_2 inversions are sharply focused on quantifying land and ocean biospheric sources and sinks because of the significantly larger uncertainties in *a priori* biospheric fluxes of CO_2 and transport models than global $ffCO_2$ emissions, together with the reality that current global carbon observing systems have been mostly designed to provide constraints on biospheric fluxes (e.g., Gurney et al., 2003, 2004; Peylin et al., 2013; Schuh et al., 2019). In light of this, global $ffCO_2$ emissions are typically not constrained in these inversions, although their importance has long been pointed out, often in the context of terrestrial and oceanic CO_2 flux inversions (e.g., Gurney et al., 2005; Peylin et al., 2011; Saeki and Patra, 2017; Gaubert et al., 2019). As discussed in Andres et al. (2012), the uncertainty in current global bottom-up fossil fuel CO_2 ($ffCO_2$) emission inventories is about 10% globally and ranges from a few percent to greater than 50% regionally (or nationally). Combustion activity and efficiency and fuel-use mixtures are still poorly characterized particularly in rapidly developing nations. This is because of the paucity of detailed information on energy use, combustion practices, and pollution control strategies in these regions (e.g., Quillcaille et al., 2018; Andres et al., 2016; Hogue et al., 2016). Most recently, Basu et al. (2020) reported that even at national level, $ffCO_2$ emission inventories in the United States are significantly underestimated by 2 to 3–*sigma* uncertainties. While significant efforts on improving bottom-up $ffCO_2$ emission inventories through detailed accounting on other sources of information have been made (e.g., Gurney et al. 2009; Rayner et al., 2010; Asefi-Najafabady et al., 2014), the lack of finer scale measurements to verify these inventories remains to be addressed. Recent reports have recognized this limitation and recommend augmenting the current observing system with systems that can help identify dynamical, physical, and chemical signatures of $ffCO_2$ at regional scales (e.g., Ciais et al., 2015).

Observational constraints on $ffCO_2$ from radioactive tracer ^{14}C have largely been established. Measurements of ^{14}C of CO_2 are able to separate the fossil and biogenic contributions in observed CO_2 and serve as useful tracer of $ffCO_2$ emissions from different regions (e.g., Levin et al., 2003, 2008; Turnbull et al., 2006, 2009, 2011, 2015; Graven et al., 2009, 2018; Miller et al. 2012; Basu et al., 2016; Niu et al., 2016; Berhanu et al., 2017; Nathan et al., 2018; Basu et al., 2020). Fossil C is ^{14}C free due to the much shorter half-life of ^{14}C (~5,700 years) than the age of the fossil (~/>10^6 years). Measurements of radiocarbon content (^{14}C) of atmospheric CO_2 may sensitively indicate fossil fuel CO_2 (delta value of -1000 ‰) additions to the air sample, showing ^{14}C is lower than contemporary background (clean air) $\Delta^{14}C$ values. While extremely useful, such measurements have only been made routinely in few locations around the world (e.g., Turnbull et al., 2007 at some Global Atmospheric Watch (GAW) sites; Berthanu et al., 2017 in Switzerland) or occasionally at specific region during field measurement campaigns (e.g., Turnbull et al., 2012 during INFLUX: Indianapolis Flux Experiment). These are still limited in providing sufficient top-down constraints on $ffCO_2$ emissions at a regional to global scale, especially emissions from poorly

https://doi.org/10.5194/acp-2020-864
Preprint. Discussion started: 31 August 2020


Atmospheric Chemistry and Physics Discussions

observed developing regions of the world. The utility of these measurements in constraining $ffCO_2$, in the context of deploying a potential network of these measurements within a joint inversion framework, have recently been assessed, albeit only through observing system simulations experiments or OSSEs (e.g., Basu et al., 2016; Nathan et al. 2018; Wu et al., 2018; Wang et al., 2018). The recent study by Basu et al. (2020) using real $\Delta^{14}CO_2$ from NOAA sites in the United States, however, shows very promising results on $ffCO_2$ emission constraints at national level. A consistent finding among these studies is that, while there is strong potential to reduce national $ffCO_2$ uncertainties (1% on yearly basis to 5-10% on monthly basis), such atmospheric-based approach to estimate emissions also requires careful consideration of errors in transport, systematic bias and accuracy of measurements, and characterization of background CO_2.

It is particularly appealing to consider synergies between CO_2 and $ffCO_2$ and air quality monitoring (AQ) observations (e.g., CO, NO_2), since in an environment where combustion activities are dominant, these species being monitored regularly often share the same dominant source category. Both are co-emitted during carbonaceous-fuel (fossil fuel-FF or biofuel-BF) generation, combustion, and distribution processes. In particular, CO is produced when combustion is incomplete; otherwise carbon in the fuel is oxidized to CO_2 at equilibrium levels of CO. And so, observing the relative abundance of $ffCO_2$, CO_2, and CO in this environment should provide useful synergistic information on their associated combustion-related emissions. This is the case for CO, for which larger number of observations are available from ground network, airborne, and satellite-derived measurements. Such datasets have been utilized in the past to provide additional constraints on combustion-related emission patterns in urban regions and biomass burning activities at local to global scales. They have been extended to provide insights on $ffCO_2$ or fire CO_2 (e.g., Suntharalingam et al., 2004; Palmer et al. 2006; Wang et al., 2010; Turnbull et al., 2011; Brioude et al., 2013; Lopez et al., 2013; Silva et al., 2013; Konovalov et al., 2014; Lindenmaier et al. 2014; Ammoura et al., 2016; Bowman et al., 2017; Super, 2018; Nathan et al., 2018; Boschetti et al., 2018 among others), as well as to identify and characterize air masses (e.g., Halliday et al. 2019). These studies used CO as an indirect tracer of combustion through a variety of ways: data analysis, model-data comparison, modeling, or inversions at different scales and region depending on their application. $ffCO_2$ emissions in bottom-up emission inventories are calculated using information on combustion activity, emission factor, and combustion efficiency (CE). A typical indicator of combustion efficiency is the ratio of measured CO_2 to ($CO + CO_2$). Differences in CE across different source sectors (e.g., power plant: high CE, domestic heating: low CE, flaming fire: high CE, smoldering fire: low CE) can be distinguished with atmospheric measurements of CO and CO_2. In particular, derived $CO:CO_2$ enhancement ratios near a source region are used to verify bulk $CO:CO_2$ emission ratios from these inventories. Hourly $ffCO_2$ emission profile from traffic are also deduced from measurements of CO (e.g., Vogel et al., 2010; Super, 2018). Because of its medium-length lifetime (1 to 2 months), CO is also a useful tracer of pollution (incl. $ffCO_2$) transport. Tracking urban plumes using CO can help enhance horizontal and vertical transport signatures of $ffCO_2$ plumes, which may be difficult with CO_2 measurements alone due to its longer lifetime and the influence of a large biospheric signal.

From a spatiotemporal sampling standpoint, these CO datasets are strongly complementary, especially in the absence or lack of CO_2 and $^{14}CO_2$ measurements. In addition, identifiable physico-chemical constraints from CO on anthropogenic CO_2 emissions and their transformations can also be exploited (i.e., oxidation of reduced carbon to CO_2, Suntharalingam et al., 2005; Nassar et al., 2010; Wang et al, 2020). In fact, the recent study by Wang et al. (2020) highlighted the

https://doi.org/10.5194/acp-2020-864
Preprint. Discussion started: 31 August 2020

Atmospheric Chemistry and Physics Discussions

impact of accounting for the chemical production of CO_2 on estimates of global carbon sinks. Yet, unlike $^{14}CO_2$, these types of information from CO are generally confounded by: a) sharp differences in their associated sinks (through chemical transformation) downwind of its source; and hence differences in lifetimes and background concentrations across space and time; b) biogenic sources even within an urban environment; and c) variations in the effectiveness of pollution control strategies for CO between sectors within an urban region. Note that many of these confounding factors become more dominant at finer scales of the study region. Hence, constraints on $ffCO_2$ emissions from CO data has to be exploited at appropriate scales. The joint inversion of CO and CO_2 by Palmer et al. (2006), for example, clearly shows that estimates of anthropogenic CO_2 can be very sensitive to assumptions of the relationship between CO and CO_2, which can then also influence the accuracy of biospheric flux estimates. Due to these factors, its use in constraining regional to global $ffCO_2$ emissions remains to be limited, despite its complementarity and the availability of a large number of its measurements. In our view, it is critical to first understand and better characterize the observed and modeled relationship between CO and CO_2 abundance before incorporating such information at appropriate scales in systems directed towards improving our capability to attribute the sources of $ffCO_2$.

1.1 Objectives

The main goals of this study are to assess the relationship between CO and CO_2 that can be inferred from observations and a climate-chemistry model and demonstrate its implications to joint CO:CO_2 inversion. Here, we take advantage of $^{14}CO_2$, CO_2, and CO measurements during a recent field campaign conducted over Korea on May 1-June 10, 2016. This study is a continuation of our work on evaluating the Copernicus Atmosphere Monitoring Service (CAMS) CO and CO_2 high resolution forecast and analysis products during Korea-United States Air Quality (KORUS-AQ) field campaign (Tang et al., 2018). This also serves as a complementary study to our recent work on quantifying the source contributions of CO over Seoul during KORUS-AQ using regional tags or tracers in the Community Atmosphere Model with Chemistry or CAM-chem (Tang et al., 2019a), and to the study by Halliday et al. (2019) on characterizing air masses using short-term CO:CO_2 ratios during the same field campaign.

The specific objectives of this study are three-fold: 1) We introduce and evaluate a single-model analysis framework for multi-species analysis and inversions; 2) We examine the modeled and observed spatial distribution of the inferred relationship between CO, $ffCO_2$ and CO_2; and 3) We demonstrate the role of CO in refining observational constraints in regional $ffCO_2$ emissions through Bayesian synthesis inversions. This framework is directed towards simulating the abundance of CO and CO_2 in CAM-chem, based on observationally constrained surface fluxes for CO_2 from global flux inversions and a 'best emission scenario' for CO from our previous work. In addition, we added a capability in CAM-Chem to tag the regional sources of ffCO and $ffCO_2$, which we could not do in our previous study using the CAMS operational forecasting system. These tags enable us to assess the relationship of regional $ffCO_2$ and CO_2 which would not be possible in this type of model using observations of $ffCO_2$ and CO_2 alone. We note that the system approach we are suggesting in this work is similar to previous global studies of these species, particularly with Palmer et al. (2006), which also considered aircraft measurements from a field campaign conducted in 2001 over similar (albeit larger) region (TRACE-P: TRAnsport and Chemical Evolution over the Pacific, Jacob et al., 2003). We view this work to be complementary to their study by updating the state of CO:CO_2 ratios in this region after 15 years. We emphasize

https://doi.org/10.5194/acp-2020-864
Preprint. Discussion started: 31 August 2020

Atmospheric Chemistry and Physics Discussions

that our focus, however, is to characterize these ratios in the context of refining $ffCO_2$ constraints, and not purely in optimizing global flux inversions. The main difference in modeling framework between this work and previous studies is the use of *a posteriori* fluxes (and emissions), rather than *a priori* fluxes in simulating the abundance. Also, while Halliday et al. (2019) and Tang et al. (2018) have already presented such characterization of $CO:CO_2$ ratios during KORUS-AQ, this study is unique in a way that we use the tagged $ffCO_2$ component of this system to attribute the contributions of regional $ffCO_2$ on these ratios.

This paper is structured as follows. In Section 2, we describe the model and datasets used in this study. In Section 3, we evaluate the modeled CO, CO_2, and $ffCO_2$ during KORUS-AQ. We characterize the spatial distribution of CO and CO_2 relationships and its implication to $CO:CO_2$ inversion in Sections 4 and 5, respectively. We present the discussion and general implications of this study in Section 6 and our conclusions in Section 7.

2. Methods and data description

2.1 CESM/CAM-Chem

The Community Earth System Model version 2 (CESM2) includes atmosphere, land, ocean, land ice, sea ice, and river components, all of which are connected by a coupler (Danabasoglu et al., 2020). CAM-chem is the atmospheric chemistry component of CESM, coupled with the land model (Lamarque et al., 2012). In CESM2, CAM-chem includes a significantly updated tropospheric chemistry mechanism (MOZART-T1), coupled to a VBS (volatility basis set) scheme for the formation of Secondary Organic Aerosols (SOA), allowing to simulate explicitly the tropospheric and stratospheric composition (Emmons et al., 2020; Tilmes et al., 2019).

2.1.1. CO_2 fluxes and CO emissions

The default CAM-chem configuration for greenhouse gases (CO_2 and CH_4) simulations are carried out by prescribing mixing ratios of these species at the model surface layer, following the CMIP6 protocol (Meinshausen et al., 2017). The CO_2 mixing ratios at the surface layer are based on zonally averaged observed CO_2 from NOAA ESRL Carbon Cycle Cooperative Global Air Sampling Network (Dlugonkencky et al., 2015). In this study, however, we simulate atmospheric CO_2 explicitly with an ensemble of external CO_2 fluxes. Specifically, we use the *a posteriori* fluxes from CAMS Greenhouse Gases (GHG) flux inversion (CAMSv17r1; Chevallier et al., 2005, 2010, 2013, 2018), CarbonTracker 2017 (CT2017; Peters et al., 2007, with updates documented at http://carbontracker.noaa.gov), and CarbonTracker Europe 2018 (CTE2018; van der Laan-Luijkx et al., 2017). CarbonTracker is a global modeling system of CO_2 developed by NOAA with a nested grid on North America (Peters et al., 2007, with updates documented at http://carbontracker.noaa.gov). CarbonTracker Europe is developed based on CarbonTracker (van der Laan-Luijkx et al., 2017). Both CT2017 and CTE2018 provide fluxes of fossil fuel, fire, land, and ocean components, which we use for our tagging of regional sources of $ffCO_2$. CAMSv17r1 is produced by the inversion system called PyVAR (Chevallier, 2018). We regridded all these CO_2 fluxes to match our CAM-chem resolution (0.95°×1.25°). Details of the fluxes are listed in Table 1 (and Table S1). Technical details for simulating atmospheric CO_2 explicitly with external CO_2 fluxes in CAM-chem are included in the supplementary material (Text S1). The term "CAM-chem CO_2", "simulated CO_2" and "modeled CO_2" in this study stand for the atmospheric CO_2 simulated

https://doi.org/10.5194/acp-2020-864
Preprint. Discussion started: 31 August 2020


Atmospheric Chemistry and Physics Discussions

with the aforementioned method rather than the atmospheric CO_2 prescribed in CAM-chem by default, unless stated otherwise. To simulate CO in CAM-chem, we use the Fire INventory from NCAR (FINN; Wiedinmyer et al., 2011) for biomass burning CO (as well as other related species such as NMVOCs) emissions, and the Hemispheric Transport of Air Pollution version 2 inventory (HTAPv2; Janssens-Maenhout et al., 2015) for anthropogenic CO (as well as other related species such as NMVOCs) emissions. In our previous evaluation of CO (Tang et al., 2019a), we calibrated these HTAPv2 emissions by doubling its associated CO and VOC emissions in East Asia and Korea to match the CO data in the region. The CT2017 CO_2 fluxes and CO emissions are shown in Figure 2 while the other 3 CO_2 fluxes and the ensemble standard deviation are shown in Figure S1.

2.1.2 Implementation

We run four CAM-chem simulations with simulated CO_2 as well as full chemistry (e.g., CO, O_3) for the year 2016, using four sets of CO_2 fluxes as described in Table S1 (including CT2017 3-hourly fluxes, CT2017 monthly fluxes, CTE2018 fluxes, and CAMS fluxes). We run CAM-chem with the model meteorological fields nudged towards Modern-Era Retrospective analysis for Research and Applications, Version 2 (MERRA-2, Gelaro et al., 2017). The CAM-chem CO_2 is initialized with CT2017 mole fraction fields on January 1st, 2016, while other variables in CAM-chem (e.g., CO) are initialized with results from previous CAM-chem simulations. The associated global budgets for our CO and CO_2 simulations are presented in Table S2. We also show in the supplementary material (Figure S2) the corresponding global CO_2 abundance for each flux product that we used and the concentration fields from CT2017. This is intended to ensure that: a) CAM-chem reasonably reproduces the CT2017 CO_2 fields when using CT2017 fluxes; b) appropriate accounting of each tag is carried out; and c) mass is conserved. Overall, our simulation results produce CO_2 fields comparable to current CO_2 analyses while carbon is reasonably accounted for. Differences in CO_2 mass is ~0.001% of initial burden which may be attributed to a cutoff of model top at ~2 hPa. In most of our analysis, we will use CAM-chem with CT3h fluxes as our base simulation. Comparisons of simulated CO_2 between other fluxes are only intended to show the total spread and not necessarily to draw conclusions on emissions or performance of these fluxes since these fluxes vary in spatiotemporal resolution.

2.1.3 Tagging $ffCO_2$ and CO

As previously noted, we developed a capability in CAM-chem to tag different source regions and/or emission types for $ffCO_2$ in addition to the existing CO tagging mechanism. This tagging approach is further described in Appendix A. We run one tagged simulation for May to June 2016 (the KORUS-AQ campaign period) using the same model configuration but only with CO_2 fluxes and CO emissions from the tagged regions defined in Figure 1. Note that for this particular simulation, we use CT2017 3-hourly fluxes for CO_2 (CT3h) and a relatively well performing CO emission scenario from Tang et al. (2019a) which is based on HTAPv2 for anthropogenic CO emissions. We tag $ffCO_2$ from 11 regions in East Asia (shown in Figure 1) with one additional tag that accounts for fossil fuel emissions from the rest of the world (ROW), to complete the $ffCO_2$ budget in CAM-chem. The CO_2 and CO tags are initialized with zero fields on Jan 1, 2016, so that only the emissions in 2016 are accounted when analyzing the relationships between $ffCO_2$ tags, CO and CO_2. Note that this Eulerian tagging method will be used to account for the relative contribution of different source regions to modeled CO_2. This is similar, in principle, to forward

https://doi.org/10.5194/acp-2020-864
Preprint. Discussion started: 31 August 2020

Atmospheric Chemistry and Physics Discussions

and backward Lagrangian trajectory models of air parcels like FLEXible PARTicle dispersion model (FLEXPART, Stohl et al. 2009) used in Turnbull et al. (2011).

2.2 Observational datasets

While we focus our analysis on KORUS-AQ measurements, we also use other datasets to assess the overall consistency of simulated CO and CO_2 (incl. their relationships) during this period. Please see the supplementary material (Table S3) for more information.

2.2.1 Aircraft measurements of CO, CO_2, and $ffCO_2$ during KORUS-AQ

The Korea United States Air Quality (KORUS-AQ) field campaign was conducted over South Korea and its surrounding waters from May to June 2016 (Al-Saadi et al., 2014; https://www-air.larc.nasa.gov/missions/korus-aq/). The flight tracks are shown in Figure 1. The Atmospheric Vertical Observations of CO_2 in the Earth's Troposphere (AVOCET; Vay et al., 2011) and Differential Absorption CO Measurement (DACOM; Sachse et al., 1987, 1991) were onboard the NASA DC-8 aircraft to measure CO_2 and CO, respectively. AVOCET uses a modified LI-COR 6252 instrument with time response of 1 second, precision and accuracy of 0.25 ppm (Vay et al. 2003). The DACOM instrument has a time response of 1 second, precision of 0.4 ppb and accuracy of 2%. These instruments were calibrated in flight during the campaign with standards from NOAA ESRL traceable to WMO CO_2_X2007 (Zhao & Tans, 2006) and CO_X2014A (NOAA, 2020).

In addition, 46 radiocarbon ($^{14}CO_2$) samples have also been collected onboard the NASA DC-8 aircraft during KORUS-AQ campaign with WAS (Whole Air Sampler team at UCI) flask samples and measured at W.M. Keck Carbon Cycle Accelerator Mass Spectrometer lab at UC, Irvine. $ffCO_2$ calculation from ^{14}C of CO_2 followed the approach by Turnbull et al. (2011), Miller et al. (2012), and Lehman et al. (2013). In particular, we use Eq. 1 of Turnbull et al. (2011) to derive CO_{2ff} (using their notation) with a background value of $\Delta^{14}CO_2$ (or Δ_{bg} in their notation) of 15‰. This value is adopted based on $\Delta^{14}CO_2$ data in Point Barrow, AK (13.9±1.5 ‰) and Niwot Ridge, CO (NWR, ~15 ‰) during the same May-June 2016 period corresponding to the KORUS-AQ campaign. This choice follows in the same manner to the discussion in Turnbull et al. (2011) on representative background values. As they pointed out, the high-altitude clean air sites, like NWR, appear to be representative of Northern Hemisphere midlatitude background and similar to Jungfraujoch, Switzerland which was also previously used in other studies to represent the background. They also pointed out that differences on the choice of background values do not significantly affect their results since these differences are smaller than the enhancements in their study region (Tae-Ahn Peninsula, Korea -TAP, Shangdianzi, China - SDZ), which is similar to our study region. In fact, we find that $\Delta^{14}CO_2$ during the campaign are always lower than 15‰. For the correction of the other effects, such as heterotrophic respiration and biomass burning (see 2nd term of Eq 1 in Turnbull et al., 2011, bias β in Eq 4 of Turnbull et al., 2009), we use -0.5 ppm corresponding to their estimate of this correction for summer months. We also follow a similar reasoning regarding the relatively small (with some that are not quantifiable in North Korea nuclear facility) ^{14}C influence on emissions of $ffCO_2$ from nuclear powerplant activities in Korea, since all the powerplant sites are using pressurized water reactor ((https://www.world-nuclear.org/information-library/country-profiles/countries-o-s/south-korea.aspx). In the same

https://doi.org/10.5194/acp-2020-864
Preprint. Discussion started: 31 August 2020


Atmospheric Chemistry and Physics Discussions

manner, the 1-*sigma* uncertainties in $ffCO_2$ and $\Delta^{14}CO_2$ are estimated to be 1 ppm and ±1.8‰, respectively.

2.2.2 Satellite-derived measurements of CO and CO_2

To provide a broader spatial context, we use retrievals of CO_2 column-averaged dry-air mole fraction (XCO_2) from the NASA Orbiting Carbon Observatory-2 (OCO-2), version 8, level 2 (L2) Lite product with the recommended quality flag (i.e., xco2 quality flag equals to 0) (Boesch et al., 2011; Osterman et al., 2017; O'Dell et al., 2018). The uncertainty of XCO_2 retrievals is about 1-2 ppm (Wunch et al., 2017). For CO, we use total column retrievals (XCO) of the Measurements Of Pollution In The Troposphere onboard Terra, version 7, Level 2, multispectral (thermal infrared/near infrared; TIR/NIR) (MOP02J, L2, V7) with the recommended quality flag (i.e.: cloud mask from MOPITT and Moderate Resolution Imaging Spectroradiometer agree on clear for Cloud Description; sum of Retrieval Anomaly Diagnostics equals to 0; solar zenith angle is less than 80) (Worden et al., 2010; Deeter et al., 2017). The model equivalent is calculated by first interpolating the model profile to the location of the satellite retrieval and applying the associated *a priori* profile and averaging kernel.

3. Comparison of modeled and observed CO, CO_2, and $ffCO_2$

A comprehensive summary of our comparison against KORUS-AQ (and other types of observing platforms) is presented in Table 2 (and Table S4). Overall, these simulations show relatively good agreement. The error statistics are comparable with state-of-the-art CO_2 and CO model simulations. The CO_2 simulations, in particular, closely matches with CT2017 mole fractions. The bias in modeled CO_2 against observations are also within the range of biases in other models. For example, the bias in CAM-chem against TCCON Saga site (Shiomi et al., 2017) range from -0.6 to -1.5 ppm, which is within the error range of OCO-2 MIP CO_2 (Crowell et al. 2019) for the same period. We emphasize here that the statistics of such comparisons (including error statistics like bias, root-mean-squared-error, and correlation) are estimated for instantaneous data points during the KORUS-AQ period (May to June 2016) or only for a single year in 2016 (in the case of NOAA and TCCON comparisons, see Figure S3 and S4). This period corresponds mostly to the peak in global average CO_2 in 2016 (Figure S2). Error comparison with other models should be limited to this specific month and year.

As shown in Figure 2, the mean spatial covariation of major sources of CO_2 and CO in the region (Beijing, Shanghai, Guangzhou, Seoul, Tokyo) for this period are broadly similar. However, they are more pronounced in observed XCO_2 than XCO. We attribute this to relatively lower sensitivity of MOPITT retrievals near the surface and differences in the source magnitudes between large cities in East Asia and Korea and Japan. While the overall correlation (R=0.46-0.68) and bias (~0.5 to 0.8 ppm) between modeled and observed XCO_2 are relatively moderate, the modeled XCO_2 is slightly underestimated in source regions (e.g., Beijing, Tokyo, Seoul) and overestimated in the Yellow Sea and northern latitudes. The modeled XCO, on the other hand, appears to be overestimated across the East Asian domain (i.e., R=0.76, bias~6.4 ppb) with higher variability (27 ppb) than observed (19 ppb). This is most likely due to the previous scaling (doubling) of anthropogenic CO and VOC HTAPv2 emissions in East Asia and Korea, as well as possible overestimation of fires in the region from FINN. Observed "background" of XCO_2 (401.75 ppm) and XCO (80.01 ppb) are slightly overestimated (402.94 ppm) and underestimated (79.50 ppb) by

https://doi.org/10.5194/acp-2020-864
Preprint. Discussion started: 31 August 2020


Atmospheric Chemistry and Physics Discussions

CAM-chem. "Background" is broadly defined here as 5th percentile across the domain for the May 2016 period. On the other hand, the 95th percentile of observed XCO_2 (408 ppm) and XCO (137 ppb), broadly representing "polluted" conditions, are underestimated (407 ppm) and overestimated (156 ppb) by CAM-Chem suggesting variations in overall bias between "background" and "polluted" conditions in this region.

3.1 Comparison against KORUS-AQ CO and CO_2 measurements

Similar to Tang et al. (2018), we organized these aircraft measurements into five flight groups to facilitate a more detailed comparison of the spatial distribution of CO and CO_2 in the region. These groups represent variations in sampling of air mass characteristics during the campaign (see Figure 3f). In particular, the Seoul flight group represents air samples over Seoul, which is characterized to have a dominant signature from anthropogenic combustion processes, while Taehwa represents air samples that may have both biospheric (nearby forest) and anthropogenic (Seoul metropolitan) influence. The flights over the West Sea were designed to capture China pollution outflows by conducting only on days when a China outflow is expected to be present. The Seoul–Jeju flight group represents air samples over local power plants, transported air from the West Sea, and over nearby croplands, while the Seoul–Busan flight group represents air samples over forest, rural, and Busan urban regions.

We show in Figures 3 and 4 the average horizontal and vertical distribution of observed and modeled CO and CO_2 for different flight groups. The overall statistics, which are calculated across all data points within a flight group, are also summarized in Table 2. For comparison with CAM-Chem CO_2, we also show the model equivalent CO_2 from the mole fractions reported in CT2017 system, which uses a different transport model (TM5). It is evident from these comparisons, that while the spatial gradients in observed CO_2 are relatively captured by CAM-chem (albeit also showing lower variability than observed), there appears to be a low negative bias (i.e., model minus obs) in nearby source regions (Seoul and its west coast), and over West Sea. The range of observed CO_2 values across flight groups, altitude, and KORUS-AQ period starts from a low of 408 ppm (Taehwa) to a high 415 ppm (Seoul) with the standard deviation ranging from 4 ppm (Seoul-Busan) to 13 ppm (Seoul). The model equivalents are slightly lower and less variable: 408 ppm (Taehwa) to 412 (Seoul) with standard deviation between 3.5 ppm (West Sea) and 10.5 ppm (Seoul). Such a slight underestimation is shown to occur in the lowermost layer of the observed CO_2 vertical profiles (Figure 4) where the median bias and interquartile range (IQR) across flight groups is -2.7±4.6 ppm. Yet over the southern coast of Korean peninsula, as well as the transect from Seoul to Busan, there is a positive bias. A slight overestimation can also be seen in the air aloft (Taehwa, Seoul-Busan, and Seoul-Jeju), where the median bias and IQR is 0.6±0.6 ppm. Above 3 km, the 5th percentile of CO_2 data (All flights) is 403.5 ppm, while its model equivalent is 405.1 ppm. Such underestimation and overestimation are consistent with our comparison against OCO-2 XCO_2 indicating variations on the influence of local and regional "pollution" (underestimation) and "background" (slight overestimation) on these biases. Differences between CAM-chem and CT2017 CO_2 are small except in below 2 km. The median difference in bias between CAM-chem and CT2017 across flight groups and altitude is -0.1±0.6 ppm, where much of the variability comes from West Sea. Since both systems use the same flux distribution (CT3h), we mostly attribute this difference to the coarser resolution (3° x 2°) of the CT2017 mole fraction fields that we obtained from Carbon Tracker, which may not be able to better represent local variations in CO_2. It is quite possible that these differences are due to differences in boundary layer

https://doi.org/10.5194/acp-2020-864
Preprint. Discussion started: 31 August 2020

Atmospheric Chemistry and Physics Discussions

representation due to coarser vertical resolution and/or different treatment of boundary layer processes between TM5 and CAM-chem. The overall bias in CAM-chem (-1 ppm) is also comparable (albeit opposite in sign) to the bias in CAMS forecast and analysis system (0.8 to 2.2 ppm) that we reported in Tang et al. (2018). This system is based on the Integrated Forecasting System (IFS) of the European Centre for Medium-Range Weather Forecasts (ECMWF) combined with modules for atmosphere composition (Flemming et al., 2017, Agustí-Panareda et al., 2017), biospheric CO_2 fluxes from terrestrial vegetation (Boussetta et al., 2013), four-dimensional variational data assimilation (Inness et al., 2019), and biogenic flux adjustment (Agustí-Panareda et al., 2016). Note that the CO_2 fluxes in this system are different from GHG CAMSv17r1 (Chevallier, 2018), which we used as one of *a posteriori* CO_2 fluxes in model. Unlike in CAM-chem, where we see an underestimation of CO_2 in the boundary layer, the positive bias in CAMS is systematic across the vertical profiles for all flight groups, except over West Sea (see Figure 4 of Tang et al. 2018).

In contrast to our comparison with MOPITT XCO across East Asian domain, the modeled CO over Korea during KORUS-AQ is generally underestimated (model minus obs: -20 to -35 ppb), except over the west of Seoul and southern Korea. The range of observed CO values across flight groups, altitude and KORUS-AQ period starts from a low of 163 ppb (Taehwa) to a high of 266 ppb (Seoul) with the standard deviation ranging from 64 ppb (Seoul-Busan) to 143 ppb (West Sea). The model equivalents are lower and less variable: 143 ppb (Taehwa) to 237 (Seoul) with standard deviation between 62 ppb (Seoul-Busan) and 133 ppm (Seoul). This is reflected in the CO vertical profiles, where across most of flight groups (except Seoul-Busan) the modeled CO is underestimated below 2 km (median bias and IQR across flight groups is -41 ±24 ppb) and above 3 km (-12 ±13 ppb). The only overestimation in modeled CO (median bias of +3 ppb), which is also reflected in the higher variability of the bias (IQR=84 ppb), can be found at 2-3 km aloft over Seoul (80 ppb), West Sea (67 ppb) and at 4-5 km over Seoul-Jeju (32 ppb). Above 3 km, the 5th percentile in observed and modeled CO are 97 and 86 ppb, respectively. Below 3 km, similar negative bias of ~12 ppb (420 ppb versus 432 ppb) can be found. This suggests an underestimation of CO in "background" conditions by CAM-chem across the vertical profile in the KORUS-AQ sampling domain. The regional influence at 2-3 km, on the other hand, is overestimated, as is also reflected in MOPITT XCO, which we attributed to an overestimation of "polluted" conditions in the model. The overall negative (and systematic) bias in CO is attributed to an underestimation of secondary and background CO or an overestimation of OH, since we still see an underestimation despite previous scaling of East Asia's and Korea's anthropogenic CO and VOC emissions. We expect that anthropogenic sources of CO in this region is already overestimated. This systematic bias has been reported in Tang et al. (2019a), which implies considering optimizing secondary CO and indirectly constraining CO loss due to OH together with primary CO emissions (Gaubert et al., 2020). Relative to CAMS CO, the overall mean bias against KORUS-AQ in CAM-chem (-24 ppb) is also comparable to CAMS (-20 to -25 ppb). Note that the CAMS system assimilates MOPITT XCO among other datasets into their forecasting system.

The correlations between CO_2 and CO errors (bias) are relatively moderate across all flight groups. These error correlations range from 0.36 over Seoul to 0.57 over West Sea, and 0.40 over All flights. These are lower than CAMS CO and CO_2 forecasts and analysis (i.e., 0.64-0.90 over Seoul, 0.80-0.82 over West Sea, and 0.49 -0.61 overall). Since CO_2 and CO simulations share a common transport in CAM-chem, lower error correlation in CAM-chem can be due to larger inconsistencies in representing CO_2 and CO sources and sinks in this model. And since both CO and CO_2

https://doi.org/10.5194/acp-2020-864
Preprint. Discussion started: 31 August 2020

Atmospheric Chemistry and Physics Discussions

simulations are consistently underestimating surface concentrations while the same set of simulations underestimate and overestimate concentrations aloft, respectively, this suggests that biases in regional sources and sinks are inconsistent between CO and CO_2. Although this inconsistency is expected by design since we used emissions and fluxes from different inventories and analysis system to highlight variations and potential errors in effective emission ratios, this also implies the need for accounting for these errors within a multi-species optimization approach.

3.2 Comparison against KORUS-AQ $^{14}CO_2$-derived $ffCO_2$ measurements

Figure 5 shows the horizontal (5a), vertical (5c), and temporal distributions (5d) of $^{14}CO_2$ measurements during the campaign. Sample IDs are indicated in the sample location along with approximate time stamps for a group of samples. We compare these with model $ffCO_2$, which is calculated as the sum of $ffCO_2$ abundance from the 12 tagged $ffCO_2$ emissions. We note that the model $ffCO_2$ is not exactly the same as $ffCO_2$ derived from the $^{14}CO_2$ measurements because of our assumption of initial condition (accounting for emissions from January 1, 2016). As described in section 2, $ffCO_2$ is derived from $^{14}CO_2$ using a $\Delta^{14}CO_2$ background value representative of the entire KORUS-AQ campaign period. Since these airborne measurements are taken close to the fossil fuel emission sources, and hence the variations in the $ffCO_2$ (accumulated since Jan 1st, 2016) are expected to mostly capture the spatial and temporal variations of regional $ffCO_2$ derived from $^{14}CO_2$ measurements. We expect that the tagged $ffCO_2$ outside of this region is small and can be lumped as an offset in $ffCO_2$ initial condition. Figure 5b also shows a scatter plot of $ffCO_2$ derived from the $^{14}CO_2$ measurements and $ffCO_2$ from CAM-chem. We note that there is a lack of variability in the model for low $ffCO_2$ samples (model standard deviation of 8.6 ppm), as shown by points clustering around 9 ppm by the model, in contrast to 1 to 12 ppm by the data (obs standard deviation of 13.2 ppm). This may be related to the relative coarse model resolution (0.9° ×1.25°). Despite the lack of variability in the model and the limited $^{14}CO_2$ samples, the overall correlation between $ffCO_2$ derived from $^{14}CO_2$ measurements and modeled $ffCO_2$ tags is moderate (R=0.51). We identified five (5) data points where derived $ffCO_2$ is significantly high (or low) relative to their model equivalents (i.e., >90th percentile of the variance of residual). These points are marked as red (orange) points in Figure 5b. Without these five data points, derived $ffCO_2$ and modeled $ffCO_2$ have a better correlation of 0.82 (R^2=0.67), which is significant at >99% confidence interval. Note that the average $^{14}CO_2$ values for this campaign period (May 2016), excluding these 5 points, is 13.2±9.5 ppm, while the 10th and 90th percentiles are in the order of 4.3 and 26.1 ppm, respectively. This is relatively consistent (albeit higher) with the values from Turnbull et al. (2011) at Tae-Ahn Peninsula (NOAA/TAP is west coast of Seoul), where the average CO_2ff they reported is 8.5±8.6 ppm and 0.4 and 23.2 ppm for 10th and 90th percentile across a different period (~2005-2010). The recent study by Lee et al. (2020) at Anmyeon-do (NOAA/KMA-GAW/AMY is 24 km away from TAP) reports a mean value of 9.7±7.9 ppm (with a range between -0.05 to 32.7 ppm) for the more recent period from May 2014 to May 2016. The value of $ffCO_2$ derived from interpolated values of NOAA/KMA-GAW/AMY CO_2 (417 ppm) and $\Delta^{14}CO_2$ (-15‰) fitted curves (https://www.esrl.noaa.gov/gmd/dv/iadv) is roughly around 11.8 ppm using the same assumptions of $\Delta^{14}CO_2$ in the region. We find a relatively higher value during KORUS-AQ as there are more polluted air masses sampled over Seoul and West Sea during the campaign. These relatively higher values imply a slight increase in derived $ffCO_2$ in this region. This is reflected in the trend of the

https://doi.org/10.5194/acp-2020-864
Preprint. Discussion started: 31 August 2020

Atmospheric Chemistry and Physics Discussions

fitted curves for CO_2 (increasing) and $\Delta^{14}CO_2$ (decreasing) at AMY and consistent with the analysis by Lee et al. (2020).

The regional contributions to modeled $ffCO_2$ are superimposed in the bar plots of Figure 5d. The observed and modeled CO_2 and CO corresponding to the same air samples are also shown in Figure 5d to show the relationship between CO_2, CO, and $ffCO_2$. While we will discuss this in more detail in the next two sections, we introduce these tags to point out that the main contributors to the modeled $ffCO_2$ during the campaign are the nearby source regions in East Asia and Korea. $ffCO_2$ ROW has relatively flat contribution across all samples. Including an offset of 1 ppm to account for errors in initial condition, the model exhibits a low bias of 1 ppm compared to derived $ffCO_2$. Note that $ffCO_2$ only accounts a small fraction of observed CO_2, even near large source regions like Seoul. We also note that the 2 sample points over Seoul, where the modeled $ffCO_2$ is significantly overestimated, correspond to large overestimation in CO when East Asia has relatively moderate contribution and overestimation in CO_2 when Korea's contribution is expected to be dominant. On the other hand, the 3 sample points over the west of Seoul and West Sea, where modeled $ffCO_2$ is significantly underestimated, correspond to an underestimation of CO and CO_2 regardless of the main source contributor. Again, this variation is consistent with the variation in bias in "polluted" conditions of modeled CO and CO_2 in East Asia described earlier. We attribute these differences to the following: (1) errors in initial condition of $ffCO_2$; (2) CO_2 (and CO) FF/BF emissions used in this study may be underestimated (overestimated) over East Asia and Korea; and (3) the vertical mixing may be overestimated by CAM-chem. We will further investigate these differences in section 5, where we conducted an inversion using derived $ffCO_2$.

4. Observed and modeled relationships of CO and CO_2

In this section, we present a closer look at the variations in CO:CO_2 correlation (R_{CO,CO_2}) and enhancement ratios ($\Delta CO/\Delta CO_2$) across flight groups and along vertical profiles. These ratios represent the change of CO abundance per unit change in CO_2 relative to their corresponding background values (i.e., enhancement or excess). Here, enhancement ratios refer to the slopes derived from a bivariate linear regression of CO and CO_2 data points rather than the estimates of the ratio of enhancements based on *a priori* knowledge of their background (e.g., Yokelson et al., 2013; Hedelius et al., 2018). The results in our model evaluation against KORUS-AQ measurements indicate that at near surface and near polluted conditions, both CO and CO_2 are underestimated suggesting a possible underestimation of common local processes, while aloft, CO_2 is slightly overestimated, and CO is underestimated suggesting a more dominant "background" influence. Here, we will assess if variations in R_{CO,CO_2} and $\Delta CO/\Delta CO_2$ also reflect this finding. We have broken down the statistics in Table 2, with regards to modeled and observed correlation between CO and CO_2 and their associated error correlations, into 6 (1-km) vertical layers for each flight group. We also derived the corresponding vertical profile of $\Delta CO/\Delta CO_2$ using two regression approaches: 1) ordinary least squares (OLS) regression approach with CO_2 as our predictor since it is more stable than CO, and 2) reduced major axis regression (RMA) at 95% confidence to account for errors in both CO and CO_2. The enhancement ratios in Table 2 correspond to regression slopes using RMA. We will refer to CAM-chem simulations with CT3h fluxes as the model equivalents for all our analyses.

https://doi.org/10.5194/acp-2020-864
Preprint. Discussion started: 31 August 2020

Atmospheric Chemistry and Physics Discussions

4.1 Correlation and error correlation

Figure 6 shows the vertical profiles of the CO:CO_2 statistics for each flight group during the campaign. Although we only plotted statistically significant correlation and error correlation, statistics using less than 30 data points are not considered in this analysis. It is important to note here that these statistics are only indicative of covariations in CO and CO_2. We focus our analysis on the relative differences between observed and modeled statistics. This only serves as another piece of information on the variability in CO and CO_2 relationship in the region.

Below 2 km, the modeled CO:CO_2 correlation (R^{mod}_{CO,CO_2}) is systematically lower than observed (R^{obs}_{CO,CO_2}) except at 1 km in Seoul-Jeju and Seoul-Busan. The average R^{obs}_{CO,CO_2} values across flight groups is 0.67±0.02 whereas the average R^{obs}_{CO,CO_2} is 0.47±0.16. Aloft, it is the opposite (i.e., modeled correlation is higher than observed) except in Taehwa, where they appear to be diverging along the upper layer of the vertical profile. The average R^{obs}_{CO,CO_2} value across flight groups in these vertical levels is 0.47±0.22, whereas the average R^{obs}_{CO,CO_2} is 0.55±0.32. This pattern of lower modeled correlation at the surface but higher aloft is clearly seen in West Sea, where we see the highest R^{obs}_{CO,CO_2} (0.95) against the lowest R^{mod}_{CO,CO_2} (0.11) among flight groups. The low R^{mod}_{CO,CO_2} relative to R^{obs}_{CO,CO_2} at the surface supports previous discussion that the model does not capture the observed variability in both CO and CO_2 data. Near the surface, a high R_{CO,CO_2} in both model and observations can be associated with well-correlated sources and sinks since CO, CO_2, and ffCO_2 share the same model transport representation. A low R^{mod}_{CO,CO_2} but high R^{obs}_{CO,CO_2} on the other hand, can be associated with lack of variability in the model. Similar underestimation of boundary layer R^{mod}_{CO,CO_2} (albeit notably smaller) can be found in Seoul (0.57 vs 0.79) and Taehwa (0.41 vs 0.61). Coarser spatiotemporal representation of associated sources and sinks and boundary layer processes can influence these values. In Tang et al. (2018), for example, we find that the 9-km resolution forecast/analysis of CAMS with 137 vertical levels (FC9s) led to significantly closer correlation to R^{obs}_{CO,CO_2} than its free running 16-km resolution (FC16s), except over West Sea where both FC16s and FC9s, like in CAM-chem, failed to capture the high R^{obs}_{CO,CO_2}.

On the other hand, above 2-3 km, R^{mod}_{CO,CO_2} is higher than R^{obs}_{CO,CO_2} indicating that the modeled air masses are more influenced by relatively less-aged plumes transported into the region. As we will discussed in later section, the influence of emissions to CO and CO_2 over Korea are significantly limited to the boundary layer and hence, the vertical profiles of these correlations exhibit a strong contrast on local and regional influences in the sampling region. During TRACE-P (2001), the R^{obs}_{CO,CO_2} coefficients reported by Palmer et al. (2006) using GEOS-Chem is mostly greater than 0.7 varying only within 5-10%. They observed lower R^{obs}_{CO,CO_2} aloft which they attribute to a larger influence of aged air masses from Asia. While noting that the flights during TRACE-P is farther downwind (and has a larger coverage) than KORUS-AQ flights, we see a similar pattern (albeit lower in magnitude) to R^{obs}_{CO,CO_2} during KORUS-AQ. The lower magnitudes are due to higher background values (and more variable) in KORUS-AQ than TRACE-P, following the same reasoning by Palmer et al. (2006) for relatively polluted TRACE-P samples located >30 degrees north. These differences highlight the importance of vertical information in effectively differentiating local and regional influences (and associated errors in transport versus emissions),

https://doi.org/10.5194/acp-2020-864
Preprint. Discussion started: 31 August 2020


Atmospheric Chemistry and Physics Discussions

547 especially within an inverse modeling framework (e.g., Stephens et al., 2007, Schuh et al., 2019,
548 Arellano et al., 2006, Jiang et al., 2015).

549 Vertical profiles of the error correlation between CO and CO_2 ($errR_{CO,CO_2}$) provide a
550 complementary perspective in examining biases in the model and in quantifying model-data error
551 covariances used in inverse modeling algorithms. A high $errR_{CO,CO_2}$ corresponds to a higher
552 correlation between the errors in CO and CO_2, while a low $errR_{CO,CO_2}$ indicates the presence of
553 model misrepresentation of processes on either CO_2 or CO that are not related to the other (i.e.,
554 different sources and sinks). Although the overall $errR_{CO,CO_2}$ values in CAM-chem is smaller than
555 we previously reported for CAMS, the $errR_{CO,CO_2}$ values in CAMS are also lower compared to
556 R^{obs}_{CO,CO_2}. We note that $errR_{CO,CO_2}$ values in both CAM-Chem (0.57) and CAMS (0.82) are highest
557 over West Sea among flight groups, regardless of resolution in the case of CAMS. Furthermore,
558 over West Sea, the $errR_{CO,CO_2}$ in CAM-chem near the surface (0.5 km) lies in the middle of its
559 R^{obs}_{CO,CO_2} and R^{mod}_{CO,CO_2}. Values of $errR_{CO,CO_2}$ that are closer towards R^{obs}_{CO,CO_2} are interpreted to reflect
560 errors in CO and CO_2 processes that are related (i.e., common sources and sinks). This indicates
561 that East Asian sources are clearly the dominant influence on $errR_{CO,CO_2}$ for these samples; more
562 than their associated sinks during transport, since over Yellow Sea, CO and CO_2 do not share a
563 common major sink. Differences between modeled and observed correlation can be associated
564 with coarser representation of related processes. On the other hand, over Seoul, CAM-chem
565 $errR_{CO,CO_2}$ (0.36) is smaller than CAMS (0.64). The value in CAMS is the second highest among
566 flight groups, while the value in CAM-chem is the lowest. The $errR_{CO,CO_2}$ over Seoul (0.35) in
567 CAM-chem near the surface (0.5 km) is lower than both R^{obs}_{CO,CO_2} and R^{mod}_{CO,CO_2}. Model
568 misrepresentation of unrelated processes may also be influencing these values (e.g., secondary CO,
569 non-ffCO_2). We note that the pattern in $errR_{CO,CO_2}$ along the overall vertical profile is consistent
570 (albeit lower in magnitude) with R^{obs}_{CO,CO_2} (except at 4-5 km where it follows R^{mod}_{CO,CO_2}). Patterns in
571 other flight groups cannot be compared due to incomplete statistically significant data points.

572 **4.2 Enhancement ratios**

573 Vertical profiles of modeled and observed $\Delta CO/\Delta CO_2$ are also shown in Figure 6. Like in previous
574 section, please note that data points in the profile which are not statistically significant in
575 correlation and having less than 30 points are not considered in this analysis to avoid
576 misinterpretation of results. Also, estimates of slopes derived from both OLS and RMA regression
577 are plotted in Figure 6 to show the difference due to the choice of regression algorithm. Although
578 both slope estimates follow the same pattern along the vertical profile, the slopes from OLS is
579 systematically lower by 50%. The OLS algorithm is useful in understanding patterns rather than
580 in comparing magnitudes with other studies. In OLS, $\Delta CO/\Delta CO_2$ can be expressed as the product
581 of R_{CO,CO_2} and the ratio of the respective standard deviations ($\sigma_{CO}/\sigma_{CO_2}$). As such, the difference
582 between OLS $\Delta CO/\Delta CO_2$ and R_{CO,CO_2} profiles correspond to $\sigma_{CO}/\sigma_{CO_2}$, for which such quantity
583 can be better represented in RMA regression.

584 Overall, the observed and modeled RMA $\Delta CO/\Delta CO_2$ across all altitudes are very similar, with
585 values of 13.30±0.21 ppb/ppm (~1.3%) and 13.80±0.23 ppb/ppm (~1.4%), respectively (see scatter
586 plot in Figure S6). Higher values of $\Delta CO/\Delta CO_2$ correspond to air masses that are characterized (in
587 a bulk average sense) as less efficient (i.e., high CO is associated with low temperature and less

https://doi.org/10.5194/acp-2020-864
Preprint. Discussion started: 31 August 2020


Atmospheric Chemistry and Physics Discussions

588 efficient combustion). However, it should be noted that as Halliday et al. (2019) pointed out, these
589 values when viewed as bulk efficiency, are limited only to bulk emission ratio interpretation since
590 these regressions are subject to transport and mixing processes as well. Values that are derived
591 from short-term covariations of CO and CO_2 are more useful for air mass characterization since
592 these ratios are non-stationary in both space and time. Variations across flight groups – here
593 representing non-stationarity in horizontal space --- (Seoul: 9.1, West Sea: 28.2, Taehwa: 15.3,
594 Seoul-Busan: 15.9, and Seoul-Jeju: 10.4 ppb/ppm) are also captured well by the model (Seoul:
595 12.6, West Sea: 33.7, Taehwa: 16.6, Seoul-Busan: 10.7, and Seoul-Jeju: 11.5. ppb/ppm). The
596 overall observed value of 13.30 ppb/ppm reflects the influence of relatively more efficient air
597 masses from Korea (flight groups other than West Sea) and less efficient air masses from China
598 (West Sea flight group)(see Figure S6 as well). The variability across flight groups within Korea
599 (Seoul and Seoul-Jeju versus Seoul-Busan and Taehwa) is likely due to a mixture of source
600 influences across these locations (i.e., biogenic CO sources and biospheric influence on CO_2 over
601 Taehwa and Seoul-Busan). These model values are comparable (albeit closer to observed values)
602 to values from the best simulation of CAMS (FC9s) in Tang et al. (2018).

603 Similar to the correlation profiles, the modeled $\Delta CO/\Delta CO_2$ show larger differences against
604 observed $\Delta CO/\Delta CO_2$ along the vertical profile. The observed values in All flights are 5.9, 11.8,
605 11.2, 10.8, 2.8, and 6.7 ppb/ppm for layers from 0.5 to 5.5 km at 1 km interval, respectively. This
606 variability with height was also pointed out by Halliday et al. (2019). Higher values can be seen
607 especially at 1.5-3.5 km. The differences between modeled and observed $\Delta CO/\Delta CO_2$ are also more
608 pronounced above 3 km (see All flights). It is interesting to note as well that the modeled values
609 at the surface from RMA regression in West Sea (21.6) and Seoul (11.2) are similar to observed
610 values (23 ppb/ppm for West Sea and 8 ppb/ppm for Seoul). Again, this suggests that the
611 differences in R_{CO,CO_2} found in West Sea are mostly due to misrepresentation of related processes
612 rather than unrelated processes. This is reflected in the lower slope from OLS that matches with
613 low R_{CO,CO_2}. The slopes from RMA are associated more to $\sigma_{CO}/\sigma_{CO_2}$ which indicate more of a
614 signature from sources and sinks than transport-related processes in R_{CO,CO_2}. This can be shown in
615 the overestimation of modeled $\Delta CO/\Delta CO_2$ at 2-3 km by 40 ppb/ppm in West Sea and 29 ppb/ppm
616 in All flights. This suggest an overestimation of emission ratio from regional sources (i.e., East
617 Asia). This is also reflected in the larger overestimation in CO (67 ppb and 80 ppb) at this level
618 over Seoul and West Sea (8 ppb in All flight) and only slight overestimation in CO_2 (0.4 to 1.2
619 ppm) consistent with our earlier discussion on biases.

620 Relative to other $\Delta CO/\Delta CO_2$ values reported in this region, the observed $\Delta CO/\Delta CO_2$ during
621 KORUS-AQ shows a similar bulk combustion efficiency contrast between South Korea and China
622 (i.e., 9 ppb/ppm in Seoul against 28 ppb/ppm in West Sea). During this campaign, the observed
623 $\Delta CO/\Delta CO_2$ from the ARIAs campaign over China (Benish et al., 2020) is also larger than 20
624 ppb/ppm. Fifteen years prior to KORUS-AQ and ARIAs, $\Delta CO/\Delta CO_2$ from northern China during
625 TRACE-P in 2001 was observed to be largely higher (50-100 ppb/ppm) than over Japan (~12-17
626 ppb/ppm) (Suntharalingam et al., 2004). A similar contrast (albeit weaker than TRACE-P) was
627 also reported by Turnbull et al. (2011) in terms of CO:CO_2ff ratios over Shangdianzi, China (~47
628 ppb/ppm) and South Korea (13 ppb/ppm) during winter 2009/2010. This is consistent with the
629 downward change in $\Delta CO/\Delta CO_2$ near Beijing from 34-42 ppb/ppm in 2005-2007 to 22 ppb/ppm
630 in 2008 (Wang et al., 2010) and derived $\Delta CO/\Delta CO_2$ from GOSAT/ACOS and MOPITT retrievals
631 over Seoul (~7-9 ± 0.5 ppb/ppm) and Beijing (~43 ±6 ppb/ppm) in 2010 (Silva et al., 2013). As

https://doi.org/10.5194/acp-2020-864
Preprint. Discussion started: 31 August 2020

Atmospheric Chemistry and Physics Discussions

we have previously noted, we expect that as combustion activities become more efficient in China, this contrast will decrease in recent years. Unfortunately, there are very limited measurements (even in TCCON AMY, Goo et al., 2017, and NOAA/KMA-GAW/AMY sites) that we can use to investigate these possible changes. The recent study by Lee et al. (2020) reports similar values ($\Delta CO/\Delta ffCO_2$) derived from NOAA/KMA-GAW/AMY site for air masses coming from the Asian continent (29-36 ppb/ppm) and Korea (8±2 ppb/ppm) during May 2014 to August 2016. Another recent study by Xia et al. (2020) also reports a mean $\Delta CO/\Delta CO_2$ of 21.6 ppb/ppm over Jingdezhen (JDZ) site in central China during the winter months of 2018 to 2019. Together with $ffCO_2$ data (section 3.2), there appears to be a decrease in this contrast relative to TRACE-P, possibly due to improved efficiency in both China and Korea energy and road transportation sectors. Activities, like biofuel and biomass burning, which have lower combustion efficiency, may still influence the higher ratios in China (e.g., Chen et al. 2017). However, this possibility needs to be verified with correlative measurements having sufficient spatiotemporal coverage of the region. As has been suggested in past studies (e.g., Turnbull et al. 2006; Vardag et al. 2015; Super, 2018; Halliday et al. 2019), these comparisons across flight groups, sampling locations, altitude, and time highlight the importance of understanding and properly accounting for the spatiotemporal variability of $\Delta CO/\Delta CO_2$ when estimating $ffCO_2$ emissions since differences in $\Delta CO/\Delta CO_2$ have confounding factors and cannot be directly attributed to discrepancies in emissions unless investigated appropriately.

4.3 Local and regional contributions

We use the tagged ffCO and $ffCO_2$ simulations to further elucidate the contributions of local and regional influences on inferred relationships of CO, CO_2, and $ffCO_2$ during the campaign. We show in Figure 7 the spatial distribution of modeled CO_2, CO, and $ffCO_2$ including the associated distribution of $ffCO_2$ tags at three representative vertical levels (model surface, 800 hPa or ~2 km, 500 hPa or ~5 km above sea level). We also show in Figure S7 a zoom-in version with a side-by-side comparison of CO_2 and CO and their associated tags at the surface and also across the mean vertical profile. The moderately strong relationship between surface CO_2 and $ffCO_2$ (0.82), which is evident over areas of fossil fuel and biofuel combustion, is also found in the relationship between surface CO_2 and CO (0.84). However, there is a high CO_2 signature over Seoul and EA-S that is not very apparent in CO, as has been noted in our OCO-2 and MOPITT qualitative assessment. High CO_2 signatures in the model are associated with mostly $ffCO_2$ (EA-M, EA-N) and fire (EA-S) emissions. Unlike CO_2 and $ffCO_2$, the similarity between CO_2 and CO is degraded at higher altitudes (0.66-0.68) due to regional and background influences in CO since $ffCO_2$ aloft is not affected by its surface sinks. Note that East Asian and ROW $ffCO_2$ also account for the majority of $ffCO_2$ at these levels, clearly indicating regional influences on the air aloft during the campaign. This is evident as well from the associated flight curtains of these tags relative to modeled CO_2 shown in Figure S8 (All group) and Figure S9 (West Sea group).

To quantify the contribution of local and regional influences of $ffCO_2$ to observed $\Delta CO/\Delta CO_2$, we decompose the modeled $\Delta CO/\Delta CO_2$ into four basis functions. The observed CO_2 can be represented as the sum of $ffCO_2$ abundance (or response functions) from Korea and Japan (hereinafter Kor+Jap), East Asia, and ROW $ffCO_2$ sources (or basis functions), along with other contributions (non-$ffCO_2$ and background), termed here as "Background+non-$ffCO_2$" (see Appendix A). We can then regress each response function to the observed CO and CO_2 following

https://doi.org/10.5194/acp-2020-864
Preprint. Discussion started: 31 August 2020

Atmospheric Chemistry and Physics Discussions

the approach used by Cheng et al. (2018) in decomposing the contributions of tagged CH_2O to $\Delta O_3/\Delta CH_2O$. That is,

$$\Delta CO/\Delta CO_2\Big|_{obs} \approx \sum_{i=1}^{i=4}\left(cov(basis_i, CO^{obs})/var(CO_2{}^{obs})\right) \quad \textit{Eq.}\ (1)$$

where $basis_i$ corresponds to $ffCO_2{}^{opt}_{Kor+Jap}$, $ffCO_2{}^{opt}_{East\ Asia}$, $ffCO_2{}^{opt}_{ROW}$ or $bg + nonffCO_2$. This "Background+non-ffCO$_2$" is calculated as the difference between $CO_2{}^{obs}$ and the sum of $ffCO_2{}^{opt}$. To ensure that ffCO$_2$ closely matches with derived ffCO$_2$ measurements (section 3), the tagged ffCO$_2$ abundances were optimized through a Bayesian synthesis inversion, which we will describe in the next section. An alternative to tagged simulations is the backward trajectory analysis using FLEXPART (Stohl et al. 2009), STILT (Lin et al., 2003), or HYSPLIT (Draxler et al., 1997). This has been used in past studies for a similar analysis (Turnbull et al., 2011; Vardag et al. 2015; Xia et al., 2020).

Here, we regress each response function with the CO and CO$_2$ data for each flight group and for each group of vertical bins (<1.5 km, 1.5-3.0 km, and >3.0 km), in order to examine the ffCO$_2$ contributions to the enhancement ratios discussed in previous section. These contributions are shown in Figure 8, together with the slope estimates from observations of CO and CO$_2$ using OLS regression. It is clear from this result that the influence of "Background+non-ffCO$_2$" dominates across the vertical levels, even near the surface and polluted conditions in Seoul. This can be seen across all flight groups, where the median contributions for each bin are ~74% for <1.5km, ~47% for 1.5-3 km, and ~81% for >3 km. We also find that ffCO$_2$ contributions in the West Sea flight group at 1.5-3.0 km and >3 km bins are dominated by ffCO$_2$ from East Asia (~67% for 1.5-3.0 km, ~131% for >3km), with the "Background+non-ffCO$_2$" contributing 90% at the surface and negatively (-52%) on the air aloft. The dominance of "Background+non-ffCO$_2$" suggests that the low R^{mod}_{CO,CO_2} relative to R^{obs}_{CO,CO_2}, yet consistent $\Delta CO/\Delta CO_2$ at the surface of the West Sea flight group, can be attributed to possible inability of the model to represent spatiotemporally finer variations in both non-ffCO$_2$ and background transport from East Asia, rather than inconsistency in ffCO$_2$ emission ratio for this region. However, it is clear that the air just above 2 km is characterized to be a low efficient airmass (high $\Delta CO/\Delta CO_2$), having higher R^{mod}_{CO,CO_2} than R^{obs}_{CO,CO_2} yet consistent $errR_{CO,CO_2}$ R^{obs}_{CO,CO_2} and very high East Asian influence. These conditions clearly indicate an overestimation of emission ratio in East Asia. While we are aware that ffCO$_2$ and CO emissions used in this study are taken from different emission inventories which may have caused this overestimation, this highlights a regional inconsistency between inventories.

The contribution of ffCO$_2$ from Kor+Jap is relatively small, even at the surface (<1.5km) in Seoul (29%), Seoul-Jeju (20%), Taehwa (15%), and Seoul-Busan (13%). Its contribution can also be seen at 1.5-3 km in Seoul-Busan (27%) and Taehwa (15%). Above 3 km, this influence is very minimal, even in Seoul-Busan (0.8%) and Taehwa (2%). In contrast, the contribution of ffCO$_2$ from East Asia is relatively high, even at the surface in Korea (Seoul: 12%, Seoul-Busan: 21%). Above 1.5 km, the East Asian influence over these flight groups are significant (35% for 1.5-3.0km, 20% for >3km) relative to Kor+Jap. These results strongly suggest that while regional influence can be inferred, it is critical to understand the vertical structure of these response functions and recognize the large influence of regional emissions and background on the local environment. The long-range transport of pollution into the region is known to be present. Simpson

https://doi.org/10.5194/acp-2020-864
Preprint. Discussion started: 31 August 2020

Atmospheric Chemistry and Physics Discussions

et al. (2020) also found a larger contribution of CO from long-range transport in the Seoul Metropolitan Area than CO from combustion over Seoul. The signal-to-noise for $ffCO_2$ abundance is very low compared to the biospheric fluxes, model transport errors, and source estimation methods (Schuh et al., 2019; Crowell et al., 2019). Accurately estimating $ffCO_2$ emissions at local-to-regional scales requires sufficient data coverage and precision, especially within the boundary layer. The statistics that we have presented also points to reducing representativeness and aggregation errors through the use of higher resolution models, which are expected to be able to capture the local scale variations. Although CAM-chem at current resolution (0.9 deg x 1 deg) is able to represent the regional-scale transport, the presence of confounding factors in the boundary layer limits our ability to improve the signal-to-noise and our ability to exploit all datasets given that associated errors are sensitive to sampling characteristics. These have been highlighted in current studies of potential $ffCO_2$ network (Wang et al., 2017; 2018). Furthermore, exploiting the finer spatiotemporal scale signatures of $ffCO_2$ on CO_2 data, which can serve as valuable observational constraint (e.g., Shiga et al., 2014; Liu et al., 2017), cannot be exploited at coarser resolution. Variations across the vertical has implications as well on inversions using columnar data from satellite retrievals of XCO_2.

5. Joint CO:CO_2 inversions

We saw from the results discussed above that there are spatial variations in CO_2 (and CO) attributable to East Asian underestimation (overestimation) and overestimation (underestimation) of "background" conditions. It is more complicated, however, to attribute a Korean underestimation (overestimation) as competing local processes are present. As we have demonstrated, using information on CO_2 and CO relationship provides more context to this problem in lieu of $ffCO_2$ data. To demonstrate the potential of CO data in refining estimates of regional $ffCO_2$ emissions, we conducted three sets of Bayesian synthesis inversions following what we learned from our model evaluation and analysis of CO, CO_2 and $ffCO_2$ and their associated relationships (section 3 and 4). We conducted two single-species experiments: 1) using $ffCO_2$ data, and 2) using CO_2 data, as well as, one joint inversion using both CO_2 and CO data. These inversion experiments are designed simply to quantify the broader role of CO in refining regional scale $ffCO_2$ signatures, which is expected to complement the current yet relatively sparse $ffCO_2$ observing system and the national networks proposed (e.g., Basu et al., 2016; Wang et al., 2018). We revisit the Bayesian synthesis inversion algorithm used in one of the first studies of joint regional CO:CO_2 inversion with aircraft data from TRACE-P and GEOS-Chem by Palmer et al. (2006). A recent study by Boschetti et al. (2018) used a similar method using IAGOS CO, CO_2 and CH_4 data (Petzold et al., 2015) and STILT to conduct OSSEs for global multi-species inversions. This approach has also been used in the past for single atmospheric constituent inversions (e.g., Enting, 2002; Baker et al., 2006; Wang et al., 2018). This approach begins with the assumption of a linear relationship between observation and model, i.e.,

$$\mathbf{y} = \mathbf{K}\mathbf{x} + \mathbf{e}_{\boldsymbol{y}}\,, \qquad \textit{Eq.}\ (2)$$

where $\mathbf{y}$ is a vector of observations (in our case: $ffCO_2$, CO, and/or CO_2), $\mathbf{x}$ is a vector of time averaged source strengths (or basis functions, which in our case is mainly $ffCO_2$ Kor+Jap, $ffCO_2$ East Asia and $ffCO_2$ ROW). $\mathbf{K}$ is a matrix of contribution (or response functions) calculated from our tagged simulations, and $\mathbf{e}_{\boldsymbol{y}}$ is a vector of errors associated to both $\mathbf{K}$ and $\mathbf{y}$. Assuming Gaussian unbiased error statistics on both $\mathbf{e}_{\boldsymbol{y}}$ and the error $\mathbf{e}_{\boldsymbol{x}}$ on the *a priori* source strengths having average

https://doi.org/10.5194/acp-2020-864
Preprint. Discussion started: 31 August 2020

Atmospheric Chemistry and Physics Discussions

values represented as a vector $\mathbf{x_a}$, the solution to this Bayesian problem is the maximum a posteriori (MAP) solution:

$$\hat{\mathbf{x}} = (\mathbf{K}^{\mathrm{T}}\mathbf{S_e}^{-1}\mathbf{K} + \mathbf{S_a}^{-1})^{-1}(\mathbf{K}^{\mathrm{T}}\mathbf{S_e}^{-1}\mathbf{y} + \mathbf{S_a}^{-1}\mathbf{x_a}), \quad \hat{\mathbf{S}} = (\mathbf{K}^{\mathrm{T}}\mathbf{S_e}^{-1}\mathbf{K} + \mathbf{S_a}^{-1})^{-1} \qquad Eq.\ (3)$$

where $\hat{\mathbf{x}}$ and $\hat{\mathbf{S}}$ are a *posteriori* mean and error covariance estimates, respectively. $\mathbf{S_e}$ and $\mathbf{S_a}$ are the expected observation $\langle \mathbf{e_y e_y}^{\boldsymbol{T}} \rangle$ and *a priori* source $\langle \mathbf{e_x e_x}^{\boldsymbol{T}} \rangle$ error covariance matrices, respectively. Superscript $^{\mathrm{T}}$ denotes transpose, $^{-1}$ the inverse of a matrix and $\langle\ \ \rangle$ is an expectation operator. These notations follow Rodgers (2000). Note that this approach suffers from wrong assumptions/misspecification of the error covariances, especially $\mathbf{S_e}$, which includes not only instrument/retrieval noise but more importantly errors in $\mathbf{K}$ when translating emissions to abundance (i.e., transport and vertical mixing errors in the tagged simulations). Here, we take a similar approach by Palmer et al. (2006) and Wang et al. (2017), where we estimate $\mathbf{S_e}$ from the error statistics we obtained in previous section. That is, $\mathbf{S_e}^{\mathrm{ffCO_2}}$, $\mathbf{S_e}^{\mathrm{CO_2}}$ and $\mathbf{S_e}^{\mathrm{CO}}$ are assumed to be diagonal matrices with the elements corresponding to $(\mathbf{e_y})^2 = (1\ \mathrm{ppm})^2$, $(\mathbf{e_y})^2 = (0.01\mathbf{y}\ \mathrm{ppm})^2$ and $(\mathbf{e_y})^2 = (0.2\mathbf{y}\ \mathrm{ppb})^2$, respectively. Note that the error variances in CO_2 and CO are relative quantities represented as fractions of the data magnitude. We also inflate these fractions to account for representativeness errors. In the case of joint CO:CO_2 inversion, we augment the observation vector such that $\mathbf{y} = [\boldsymbol{y^{CO_2}},\ \ \boldsymbol{y^{CO}}]^T$. We also use the error correlation between CO and CO_2 discussed in previous section. That is, $\mathbf{S_e}$ can be expressed as:

$$\mathbf{S_e} = \begin{bmatrix} \boldsymbol{I_{n_y}}(\boldsymbol{e_y^{CO_2}})^2 & \boldsymbol{I_{n_y}} errR_{CO,CO_2} \\ \boldsymbol{I_{n_y}} errR_{CO,CO_2} & \boldsymbol{I_{n_y}}(\boldsymbol{e_y^{CO}})^2 \end{bmatrix} \qquad Eq.\ (4)$$

where $\boldsymbol{I_{n_y}}$ is an identity matrix with n_y diagonal elements corresponding to the number of data points for each species. Here, we use a much lower $errR_{CO,CO_2}$ of 0.33. Notice that in Palmer et al. (2006), they used R_{CO,CO_2} (0.7) on $\mathbf{S_e}$, which is much higher than the model-dependent $errR_{CO,CO_2}$ from this study. A similar error correlation of 0.7 was also used by Boschetti et al. (2018). While we recognize that from a purist perspective, $\mathbf{S_e}$ should only account errors in the data, we also need to account for model errors (in observation space) as the assumption of perfect $\mathbf{K}$ is obviously not valid. We use the more conservative $errR_{CO,CO_2}$ to represent the correlation component of $\mathbf{S_e}$ assuming that these model errors are more reflected in correlation than the variance structure of $\mathbf{S_e}$. However, we still use the errors on the data to represent the error variance component of $\mathbf{S_e}$ but with added inflation to account for representativeness errors (which is also model-dependent). Albeit clearly simplified, this is along the same line as the more rigorous representation of these errors discussed in Wang et al. (2017, 2018) and Basu et al. (2016). We also filter the data with points having the residual (model-obs) variance that is a factor of 1.25 (for $ffCO_2$ data) or 2.0 (for CO_2 and CO data) greater than the overall residual standard deviation. More importantly, we only use data below 3 km for localization purposes (see previous section). The effective number of data points for each observation vector that are used in a particular inversion are as follows: $n_y^{fCO_2}$=41, $n_y^{CO_2}$=4,716, and n_y^{CO}=4,716. Notice that exactly the same set of CO_2 data points in CO_2 inversion is used for the joint CO:CO_2 inversion to facilitate comparison between inversions. Our emphasis for these inversions is to show the role of CO in refining our

https://doi.org/10.5194/acp-2020-864
Preprint. Discussion started: 31 August 2020

Atmospheric Chemistry and Physics Discussions

estimates of $ffCO_2$ emissions rather than accurately estimating biospheric sources and sinks. For the same reason that we use *a posteriori* CO_2 fluxes rather than the *a priori* CAM-chem fluxes.

For single-species inversion using $ffCO_2$ data, we added another basis that we call '$ffCO_2$ Offset'. This is a constant term (1 ppm) that is intended to account for a potential bias in $ffCO_2$ due to our assumption of $ffCO_2$ initial condition. We replace the basis "$ffCO_2$ Offset" for the single-species inversion using CO_2 data with the residual between modeled CO_2 and modeled $ffCO_2$ and call it "Background+non-$ffCO_2$" as noted in section 4.3. This represents the larger non-$ffCO_2$ component of CO_2 (see Eq. A.1). Both single-species inversions will have m=4 basis functions that will be optimized using Eq. 3. For joint inversion, there will be m=8 basis functions corresponding to CO_2 and CO basis (i.e., $\mathbf{x_a} = \begin{bmatrix} \boldsymbol{x_a^{CO_2}} & \boldsymbol{x_a^{CO}} \end{bmatrix}^T$). The 4x4 $\mathbf{S_a}$ matrix for single species $ffCO_2$ inversion is assumed to be diagonal with $\mathbf{e_x} = \boldsymbol{d} \circ \mathbf{x_a}$ and $\boldsymbol{d} = [0.3, 0.3, 0.1, 0.5]^T$ to account for heteroskedasticity in these errors. We assumed that error in $ffCO_2$ ROW is the smallest while the "$ffCO_2$ Offset" is largest. However, as we mentioned before, the $^{14}CO_2$-derived $ffCO_2$ is representative of the regional $ffCO_2$ (not global) and specific to the assumptions of $\Delta^{14}CO_2$. We have seen from section 4.3 as well that $ffCO_2$ ROW has negligible contributions to $\Delta CO/\Delta CO_2$ in the region. We expect that the errors in $ffCO_2$ ROW and "$ffCO_2$ Offset" to be largely correlated. Accordingly, the 8x8 $\mathbf{S_a}$ matrix for the joint CO:CO_2 inversion is constructed as follows:

$$\mathbf{S_a} = \mathbf{s} \cdot \mathbf{C_a} \cdot \mathbf{s}, \text{ where } \mathbf{s} = \begin{bmatrix} \boldsymbol{I_4}\left(\boldsymbol{e_x^{CO_2}}\right)^2 & \mathbf{0} \\ \mathbf{0} & \boldsymbol{I_4}(\boldsymbol{e_x^{CO}})^2 \end{bmatrix} \text{ and } \mathbf{C_a} = \begin{bmatrix} \boldsymbol{I_4} & \boldsymbol{I_4 c} \\ \boldsymbol{I_4 c} & \boldsymbol{I_4} \end{bmatrix} \quad \textit{Eq.} (5)$$

We assumed no correlation across basis functions within a particular species. However, the source error correlation across species is specified as $\mathbf{c} = [-0.5, -0.5, -0.1, 0.0]^T$. We also assumed that the source error correlation across species is higher near the source region (i.e., East Asia and Kor+Jap) and smaller to negligible for the more "diffused" sources from ROW and "Background+non-$ffCO_2$". At the source, CO is mostly negatively correlated with CO_2 (i.e., higher combustion efficiency is associated with low CO). It should be noted that while this vector is critical in transferring information from CO (or CO_2) data to the other species (Palmer et al., 2006, Boschetti et al. 2018), there is little information on quantifying this correlation. In fact, it is very difficult to accurately specify the elements of $\mathbf{C_a}$ since these statistics cannot be derived from measurements. There are only few direct measurements of CO_2 fluxes (and CO emissions) to quantify their associated errors. One way to estimate $\mathbf{C_a}$ is to have an ensemble of CO and CO_2 sources, where we can compute its statistics following a similar approach by Wang et al. (2018). For this study, however, we follow a simpler approach using similar critical values of these correlations suggested in Palmer et al. (2006). This is more conservative than the correlation used by Boschetti et al. (2018) of 0.7. We note that in our setup, *a posteriori* estimates are not that sensitive to the correlation values in $\mathbf{S_a}$ than in $\mathbf{S_e}$. We also specify the error variances while accounting for heteroskedasticity as: $\boldsymbol{e_x^{CO_2}} = \boldsymbol{d_{CO_2}} \circ \mathbf{x_a^{CO_2}}$ where $\boldsymbol{d_{CO_2}} = [0.3, 0.3, 0.1, 0.05]^T$ and $\boldsymbol{e_x^{CO}} = \boldsymbol{d_{CO}} \circ \mathbf{x_a^{CO}}$ where $\boldsymbol{d_{CO}} = [0.5, 0.5, 0.1, 0.05]^T$. These error variances are typically prescribed to be larger than reported 1-*sigma* uncertainties in order to include potential errors that are unaccounted for. We assumed that errors in ffCO emissions are larger in East Asia, and Kor+Jap than in ROW while the "Background+non-ffCO" is smallest based on their associated variability.

https://doi.org/10.5194/acp-2020-864
Preprint. Discussion started: 31 August 2020

Atmospheric Chemistry and Physics Discussions

5.1 Inversion results

We present in Figure 9 the results of the three sets of inversions. We show the change in *a posteriori* estimate relative to *a priori* (represented here as scaling factors) of $ffCO_2$ basis including "$ffCO_2$ Offset" or "Background+non-$ffCO_2$" (depending on the dataset used in the inversion). The error bars correspond to the square root of the diagonal elements of $\hat{\mathbf{S}}$ for *a posteriori* or $\mathbf{S_a}$ for *a priori* estimates. The error for *a priori* "Background+non-$ffCO_2$" is not shown. For $ffCO_2$ inversion, we find that $ffCO_2$ East Asia and $ffCO_2$ Kor+Jap need to be increased by ~27% ±9% and ~10% ±3%, respectively. At the same time, $ffCO_2$ ROW needs to be slightly decreased (albeit with higher uncertainty) by 14% ±9%. This results to a reduction in bias (model-obs) against $ffCO_2$ derived measurements (including "$ffCO_2$ Offset") from -1 ppm to -0.01 ppm. The error reduction in $ffCO_2$ estimates (1- $\hat{e}_x/e_x$), where $\hat{e}_x$ is the *a posteriori* error, is largest in $ffCO_2$ Kor+Jap (91%) followed by $ffCO_2$ East Asia (71%), "$ffCO_2$ Offset" (62%), and $ffCO_2$ ROW (8%), suggesting that East Asia and Kor+Jap are reasonably resolved by the measurements. Again, it is important to note that we do not expect $^{14}CO_2$-derived $ffCO_2$ measurements to resolve $ffCO_2$ ROW. The error reductions in East Asia and Kor+Jap are comparable to the uncertainty reduction (UR) values reported in Wang et al. (2018) for OSSEs using a potential $ffCO_2$ network in Europe. The increases in East Asia and Kor+Jap are also expected based on our evaluation of modeled CO_2 and $ffCO_2$ (section 3) and our analysis of CO and CO_2 relationships (section 4) of apparent underestimation of CO_2, and $ffCO_2$ below 3 km. Although such increase is reasonable and within range of the uncertainties in regional $ffCO_2$ emissions (Andres et al., 2012), the equivalent reduction of the bias in terms of CO_2 abundance remains small, even with the contribution of "$ffCO_2$ Offset". This is consistent with the relatively low contribution of $ffCO_2$ from these source regions discussed in section 4.3.

We find reasonable consistency in scaling factors that are within the range of their associated uncertainties when CO_2 and CO across the campaign are used instead of $ffCO_2$ data. In particular, emissions of $ffCO_2$ from East Asia and Kor+Jap need to be increased by ~27% ±24% and (9% ±17%). However, the scaling factor for $ffCO_2$ from ROW only suggests a smaller decrease (6%±10%) in $ffCO_2$ emissions compared to $ffCO_2$ inversion. The "Background+non-$ffCO_2$" appears to only have a very small decrease (0.7% ±0.3%). Reduction in the error estimates are lower (although still significant) in East Asia (20%) and Kor+Jap (42%). On the other hand, there is very little error reduction in ROW (0.4%) but higher error reduction in "Background+non-$ffCO_2$" (94%) indicating that the estimate of $ffCO_2$ from ROW is not resolved using either CO, CO_2 or $ffCO_2$ measurements. This is expected as the source error correlation for this basis function is smaller and that the contribution of $ffCO_2$ ROW is already very small to begin with. On the other hand, the error reduction in "Background+non-$ffCO_2$" is mostly constrained by CO_2 data given that we assumed zero source error correlation across species. However, unlike the joint inversion, we find larger differences in $ffCO_2$ mean estimates when CO_2 measurements across the campaign are used. Our results show a decrease in both $ffCO_2$ East Asia (5% ±27%) and Kor+Jap (6% ±19%) and practically no changes in $ffCO_2$ ROW (0% ±10%) and "Background+non-$ffCO_2$" (0% ±0.3%). The error reduction is slightly smaller than the reduction from joint inversion for East Asia (9%) and Kor+Jap (38%), while similar error reduction can be observed for ROW (0.1%) and "Background CO_2" (94%), again suggesting that $ffCO_2$ ROW is not resolved neither by CO_2 nor CO measurements as well.

https://doi.org/10.5194/acp-2020-864
Preprint. Discussion started: 31 August 2020


Atmospheric Chemistry and Physics Discussions

6. Discussion and general implications

These results imply that inversion using CO and CO_2 data is able to match the regional $ffCO_2$ emission estimates for East Asia and Kor+Jap from $ffCO_2$ inversion, whereas using CO_2 data alone is not sufficient even with a much larger number of data points compared to $ffCO_2$ data. This is seen in the estimates of the mean of $ffCO_2$ East Asia and Kor+Jap, where CO pulls this estimate in the same direction as the ones using $ffCO_2$ data. This adjustment is mostly due to the addition of model-data error correlation across species ($\mathbf{S_e}$) than source error correlation across species ($\mathbf{S_a}$). A suggested decrease of CO emissions in East Asia and Kor+Jap, along with an increase in "Background+non-ffCO" sources resulted to increases in East Asia and Kor+Jap $ffCO_2$ emissions. Note that our *a priori* HTAPv2 CO and VOC emissions were doubled for East Asia and Korea to begin with. The slight negative bias in CO at the surface and larger positive bias at 2-3 km, especially over Seoul and West Sea, is consistent with the adjustments in CO, indicating that bias in CO is mostly from underestimation of secondary CO and possibly ffCO ROW (e.g., India). The dominance of $\mathbf{S_e}$ on our results for $ffCO_2$ is in contrast to Boschetti et al. (2018). This may be due to our approach of localizing our data to below 3 km and aggregating to a smaller number of basis functions. Nevertheless, *a posteriori* estimates in $ffCO_2$ sources using $ffCO_2$ and CO with CO_2 data are statistically significantly indistinguishable from a two-tailed t-test at 99% confidence interval. This is not the case between *a posteriori* estimates in $ffCO_2$ sources using $ffCO_2$ and CO_2 data. We recognize that this is only a proof-of-concept to demonstrate the complementary information in CO data on $ffCO_2$ at regional scales (even with conservative use of error correlation estimates). These results are consistent with our analysis of covariation between CO, CO_2, and $ffCO_2$ during the campaign, where the regional difference between air masses from China and Korea is clearly evident. Vertical profiles of these covariations (both correlation and enhancement ratio) reveal this regional contrast.

However, the modeled local covariations are confounded by misrepresentation of local and transport-related processes. Such type of errors can skew the results and have to be addressed (e.g., Wu et al., 2018). Our analysis approach was designed to account for these confounding factors (albeit sub-optimally) by specifying relatively conservative (larger) error covariances and only using data below 3 km to mimic the sampling distribution of derived $ffCO_2$ measurements, which is used in this study as our basis of comparison. We are aware that this is still sub-optimal but detailed refinements to this approach is beyond the scope of this study. We highlight some of these limitations in Figure 10, where we show vertical profiles of $ffCO_2$ contributions from East Asia, Kor+Jap and ROW emissions, including the overall bias in CO_2 relative to DC-8 CO_2 data. While there is an apparent increase in boundary layer $ffCO_2$ over the West Sea (~1.25 ppm) from the same increase in *a posteriori* scaling factor relative to *a priori* emissions from East Asia, this increase only translates to a decrease of ~0.9 ppm in the CO_2 bias for this flight group as a result of all $ffCO_2$ adjustments since there is competing effect between a slight increase in $ffCO_2$ Kor+Jap and a decrease in $ffCO_2$ ROW. In addition, the use of a single scaling factor for a broad basis function results to a degradation of CO_2 aloft, suggesting that non-$ffCO_2$ and background CO_2 needs to be adjusted accordingly by region (not globally) since they are dominant aloft. This sensitivity between $ffCO_2$ and non-$ffCO_2$ estimates has been pointed out in previous studies (e.g., Palmer et al., 2006; Basu et al., 2016; 2020). An added complication to these inversions is the accounting of CO_2 chemical production (Wang et al. 2020) that may also be reflected in the "Background+non-$ffCO_2$". The aggregation error (Kaminski et al., 2001) confounding our results also needs to be addressed, perhaps by adding regional basis functions for non-$ffCO_2$ and

https://doi.org/10.5194/acp-2020-864
Preprint. Discussion started: 31 August 2020

Atmospheric Chemistry and Physics Discussions

background CO_2 within a multi-scale (or multi-tiered) hierarchical inversion framework (e.g., Cusworth et al., 2020). An ensemble approach using a larger ensemble size from different flux inversions (e.g., Global Carbon Project, OCO-2 MIP) may offer opportunities to better quantify the *a priori* error covariances of non-$ffCO_2$ and background CO_2. We also recognize that by design this is a simplistic study focused on CO data as potential constraints on regional $ffCO_2$. A more realistic scenario would be to show its impact on top of current observational constraints for CO_2 (e.g., XCO_2 satellite retrievals and derived $ffCO_2$ measurements). Augmenting the flux vector in CO_2 flux inversions with CO and $ffCO_2$ sources may also offer opportunities to understand its impact on biospheric flux estimates (Basu et al., 2016, 2020; Wang et al., 2020).

There have been several studies using information on local enhancement (ΔCO) that can be derived from $\Delta CO/\Delta CO_2$ to constrain $ffCO_2$ emissions (Super, 2018). This approach employs assumptions on the spatiotemporal distribution of emission ratios between CO and $ffCO_2$ using mass balance. We emphasize here that CO may not be the most appropriate data unless the stationarity assumption for these $\Delta CO/\Delta CO_2$ are valid and temporal changes in CO_2 are reasonably characterized (e.g., Nassar et al. 2013; Liu et al., 2017). This has been indicated for example in Super (2018) and Nathan et al. (2018). As has been highlighted in this study, the use of regression approach in deriving these relationships are confounded by mixing and transport-related processes making it difficult to attribute the changes in the slopes to emission ratios alone, especially when analyzing downwind measurements. For this purpose, we suggest a 'model calibration' approach where $ffCO_2$ emissions are adjusted based on CO_2 and CO tags and derived $\Delta CO/\Delta CO_2$ at a spatiotemporal scale that is representative of the best possible change in combustion efficiency. In particular, changes in $ffCO_2$ emissions due to changes in CE (through improved technology, pollution abatement, changes in fuel mixture, process changes, or even decommissioning of a power plant) do not manifest at local spatiotemporal scale. Ratios derived at finer scale can be noisy and non-stationary. Changes in emissions due to changes in CE is usually detectable at a far longer spatiotemporal scale. Long-term satellite retrievals of CO and other proxies of fossil fuel combustion signatures (e.g., NO_X) at decadal timescale (Tang et al., 2019b; Zheng et al. 2018) may be useful to detect trends on the changes of $ffCO_2$ emissions (Yin et al., 2019).

7. Conclusions

In this study, we highlight the spatial variability of tropospheric CO and CO_2 relationships and its implication in constraining CO_2 from fossil fuel combustion. We use the KORUS-AQ field campaign as our case study. This campaign, which was aimed to study air quality in South Korea, was conducted on May to June 2016. Incidentally, it also coincided with the peak in global CO_2 concentration for this particular year. We use a single-model (CAM-chem) analysis framework, where the *a priori* CO_2 fluxes in the model are taken from *a posteriori* fluxes of recent global flux inversions (e.g., Carbon Tracker – CT2017). We also use CO emissions that were calibrated with CO data (albeit in an ad-hoc manner) from our previous CAM-chem CO analysis. The availability of $^{14}CO_2$, CO, and CO_2 vertical profiles from NASA DC-8 offers an opportunity to assess the fidelity of this framework in simulating CO and CO_2 abundances from the best possible and observationally constrained fluxes and emissions. More importantly, this framework enables us to facilitate a better understanding of the variability in observed and modeled relationships between the abundances of these species. Our analysis is directed towards investigating the covariation of CO, CO_2, and $ffCO_2$, which can then be made useful in refining our estimates of regional $ffCO_2$ emissions.

https://doi.org/10.5194/acp-2020-864
Preprint. Discussion started: 31 August 2020

Atmospheric Chemistry and Physics Discussions

We evaluated CAM-chem CO and CO_2 simulations from a variety of observing system perspectives, while focusing on key diagnostics relative to KORUS-AQ measurements and previous model and data analysis for this particular period and region. Our results show that the spatiotemporal distribution of CAM-chem CO and CO_2 simulated abundances (and their associated correlations and enhancement ratios) are reasonably consistent (and within the range of uncertainties) with KORUS-AQ CO and CO_2 data, CAMS high resolution forecast/analysis of CO and CO_2, and CT2017 mole fractions for CO_2 -- both of which used different transport models at different resolution. In particular, we find that: 1) The overall biases against DC-8 CO_2 and CO measurements in CAM-chem using CT2017 fluxes are -1.0 ppm and -24 ppb, respectively, while the CAMS FC9s is biased by about 0.7 ppm in CO_2 and -17 ppb in CO. The CT2017 CO_2 mole fraction is biased by -1.2 ppm; 2) The overall correlation (R_{CO,CO_2}) and enhancement ratio ($\Delta CO/\Delta CO_2$) between CO and CO_2 are as follows: DC-8: 0.67 and 13.3±0.21 ppb/ppm, CAM-chem: 0.55 and 13.8±0.23 ppb/ppm, and CAMS FC9s – 0.65 and 12.5 ppb/ppm. The error correlation $errR_{CO,CO_2}$ in CAM-chem (0.40) is also comparable to CAMS FC9s (0.49); 3) The overall bias in CAM-chem $ffCO_2$ against $^{14}CO_2$ data is -1 ppm, which is close to 1-*sigma* uncertainty of the data (1 ppm). We also note that the modeled CO and CO_2 correlation and enhancement ratios vary differently relative to DC-8, suggesting possible misrepresentation of related sources and sinks in CAM-chem. In particular, we find a significantly lower (higher) correlation near the surface (aloft) over West Sea relative to DC-8, whereas its enhancement ratio is comparable near the surface but larger aloft. We attribute this difference to coarser representation of boundary layer processes (low correlation) and overestimation of regional emission ratio aloft (high enhancement ratio).

We also investigated the contribution of regional $ffCO_2$ to observed $\Delta CO/\Delta CO_2$ using tagged $ffCO_2$ simulations. We find that, even near the surface in Seoul, there is a significant contribution of background and non-$ffCO_2$ that cannot be neglected. Its median contribution across flight groups is 74% below 1.5 km, 47% between 1.5 and 3km and 81% > 3 km. $ffCO_2$ from East Asia also contributes significantly, with median contributions ranging from 10% below 1.5km, 35% between 1.5 and 3 km, and 20% >3 km. Its higher contribution is especially evident at all levels over the West Sea air samples, which are representative of Chinese pollution outflows. These variations in contributions affect the design and interpretation of joint CO:CO_2 inversions. We find, for example, that in order to effectively constrain $ffCO_2$ emissions from Kor+Jap and East Asia, we have to localize our inversion to data points below 3 km. Else, the larger impact of "Background+non-$ffCO_2$" can obscure the response from $ffCO_2$ emissions. We conducted three sets of inversions to demonstrate the impact of CO data in refining estimates of regional $ffCO_2$ emissions. While recognizing the simplicity of our joint Bayesian synthesis inversion (which follows Palmer et al., 2006), we find that $ffCO_2$ from East Asia and Kor+Jap need to be increased by 27%±24% and 9%±17%, respectively. This is very consistent (albeit with larger uncertainty) with results from an inversion using derived $ffCO_2$ data only (East Asia: 27%±9% and Kor+Jap: 10%±3%). In contrast, inversion using only CO_2 data results to a decrease in both East Asia (-5%±27%) and Kor+Jap (-6%±19%) reflecting the difficulty to differentiate the response of background+non-$ffCO_2$ and regional $ffCO_2$ using CO_2 profiles alone.

Although these results are promising, we emphasize that this is only proof-of-concept which needs to be refined with more rigorous and realistic inverse modeling experiments for different observing systems. This is especially the case for global inversion systems that take into account the appropriate scales inherent in these types of information and goes beyond the use of traditional

https://doi.org/10.5194/acp-2020-864
Preprint. Discussion started: 31 August 2020


Atmospheric Chemistry and Physics Discussions

error covariance estimation. CO, in particular, is useful in constraining $ffCO_2$ at regional scales since this scale is commensurate to its lifetime of 1 to 2 months. It becomes problematic at local scales due to its inherent confounding factors and inability of global chemical transport models to capture its variability at these scales. While this study focuses on a specific region, we highlight in this work the importance of rigorously verifying the relationships and sensitivities derived from regional and global models to any joint inverse analyses. It is especially important to verify consistencies across species. Careful consideration of associated errors on the vertical distribution of these sensitivities and assumptions of stationarity is warranted, especially for future joint analyses using satellite columnar retrievals of these species, which lack vertical information and may not necessarily be collocated in both space and time.

https://doi.org/10.5194/acp-2020-864
Preprint. Discussion started: 31 August 2020

Atmospheric Chemistry and Physics Discussions

Acknowledgments

This study is supported by NNX16AE16G, NNX17AG39G and NNH18ZDA001N. We also thank the CESM and CAM-chem team for technical support, including Stephanie Wuerth for sharing her CAM/DART code modifications. The CESM project is supported primarily by the National Science Foundation (NSF). This material is based upon work supported by the National Center for Atmospheric Research, which is a major facility sponsored by the NSF under Cooperative Agreement No. 1852977. Computing and data storage resources, including the Cheyenne supercomputer (doi:10.5065/D6RX99HX), were provided by the Computational and Information Systems Laboratory (CISL) at NCAR. We especially acknowledge the scientific and product teams in CarbonTracker, CarbonTracker-Europe, and CAMS GHG inversion for the CO_2 flux products that they have kindly provided. CarbonTracker CT2017 results provided by NOAA ESRL, Boulder, Colorado, USA from the website at http://carbontracker.noaa.gov. We also thank the teams involved in HTAP and FINN for CO emission inventories. We acknowledge the following teams for their great effort in taking CO_2 and CO measurements and providing them publicly: KORUS-AQ for DC-8 measurements, TCCON for XCO and XCO_2, NOAA ESRL Carbon Cycle Cooperative Global Air Sampling Network for the surface air flask sampling data, MOPITT and OCO-2 for XCO and XCO_2 retrievals, respectively. We thank Dr. Donald Blake's research group from the University of California, Irvine for collecting the airborne flask samples. The NCAR MOPITT project is supported by the National Aeronautics and Space Administration (NASA) Earth Observing System (EOS) Program. We specially thank Dr. Frédéric Chevallier and Dr. Britton Stephens for their insightful comments on improving this manuscript. All the fluxes and emissions, and observational data are available online.

Code and datasets

CESM2.0 is a publicly released version of the Community Earth System Model and freely available online (at www.cesm.ucar.edu, last access: 14 August 2020). The Korea-United States Air Quality Field Study (KORUS-AQ) dataset is available at https://doi.org/10.5067/Suborbital/KORUSAQ/DATA01. MOPITT data is available at https://www2.acom.ucar.edu/mopitt while the Orbiting Carbon Observatory-2 XCO_2 is available at https://disc.gsfc.nasa.gov/datasets/OCO2_L2_Lite_FP_9r/summary. The Total Carbon Column Observing Network (TCCON) and NOAA datasets can be downloaded at https://tccondata.org and (https://www.esrl.noaa.gov/gmd/ccgg/flask.php), respectively.

https://doi.org/10.5194/acp-2020-864
Preprint. Discussion started: 31 August 2020

Atmospheric Chemistry and Physics Discussions

Appendix A. Tagging ffCO$_2$ and ffCO in CAM-chem

The abundance of tropospheric CO_2 at any given space (s) and time (t) can be decomposed into contributions from different processes. That is,

$$CO_2(s,t) = CO_2^{bg}(s,t) + \left(CO_2^{ffbf}(s,t) + CO_2^{bb}(s,t) + CO_2^{cem}(s,t) + CO_2^{res}(s,t) + CO_2^{chem}(s,t)\right) - \left(CO_2^{lnd}(s,t) + CO_2^{ocn}(s,t) + CO_2^{st}(s,t)\right) \quad (A.1)$$

where bg denotes background, $ffbf$, bb, cem, res and $chem$ are CO_2 sources from fossil fuel/biofuel combustion, biomass burning, cement production, biospheric respiration, and chemical production processes, while lnd, ocn, st are CO_2 sinks due to biospheric (photosynthetic) uptake, ocean-tropospheric, and tropospheric-stratospheric exchange, respectively. Our notation of non-ffCO_2 corresponds to other sources that are not $ffbf$.

Similarly,

$$CO\,(s,t) = CO^{bg}(s,t) + \left(CO^{ffbf}(s,t) + CO^{bb}(s,t) + CO^{oxid}(s,t)\right) - \left(CO^{OH}(s,t) + CO^{dep}(s,t)\right) \quad (A.2)$$

where $oxid$, OH and dep denote secondary CO due to VOC oxidation, CO sinks due to its reaction with OH radical and dry deposition, respectively.

We have developed tagging capabilities in CAM-chem for both CO and CO_2 sources by prescribing their associated sinks. Tagging CO has been developed in the past by treating CO from a particular basis function as tracers. That is, we solve the continuity equation for every tagged CO in the same way as the default CO variable in the model but making sure that each tagged CO does not interact with model chemistry (i.e., by treating it as a passive tracer). This mechanism is mentioned in Emmons et al. (2012) and previously used in Bayesian synthesis inversion studies (e.g., Arellano and Hess, 2006) and chemical budget studies (Gaubert et al., 2016). A similar approach is also used by Fisher et al. (2017) with GEOS-Chemv9 model. This tagging capability is further illustrated in Eq. A.3 for a particular tag CO (*itag*).

$$\frac{\partial [X]^{itag}}{\partial t} = \frac{\partial [X]^{itag}}{\partial t}\Big|_{transport} + \frac{\partial [X]^{itag}}{\partial t}\Big|_{sources} - \frac{\partial [X]^{itag}}{\partial t}\Big|_{sinks} \quad (A.3)$$

The temporal evolution of a tracer $[X]^{itag}$ for each grid cell in the model is calculated using the same continuity equation for species $[X]$. As expressed in Eq A.2, this includes the background dynamics represented here as transport term (dynamics and physics incl. advection, diffusion, mixing, convection, and CO flux convergence and divergence), all sources (emissions and chemical production), and all sinks (CO+OH reaction, and deposition). These tags or basis can be either disaggregated sectoral components and/or regional source components of CO depending on the problem to be addressed. Here, we use ffCO emitted from a few regions around Korea as our

https://doi.org/10.5194/acp-2020-864
Preprint. Discussion started: 31 August 2020

Atmospheric Chemistry and Physics Discussions

basis. All these regions are defined in Figure 1. The response of this basis or the contribution of this source region to overall abundance in CO is estimated by integrating Eq. A.3. Hence, the simulated $[CO]^{itag}$ for example corresponds to $[CO]$ mixing ratio for a given mass of CO emitted to the atmosphere by this *itag* region. The CO tags added in CAM-chem consists of the following edits to the code: (1) The CO tags are defined in the chemical preprocessor (variable names are arbitrary defined as "CO01", "CO02" …); (2) emission files for the tags of emissions from specific regions are prepared and defined in the namelist; (3) chemical production of CO for CO tags of chemical sources are defined by adding related chemical reactions in chemical preprocessor; (4) the OH chemical loss is defined in the chemical preprocessor, OH is not affected by the oxidation of tags; (5) dry deposition for the CO tags is applied in the same way as for the default CO variable. Detailed evaluation and validation of CAM-chem CO tags can be found in Tang et al. (2019a) and https://wiki.ucar.edu/display/camchem/.

We apply a similar approach in tagging ffCO$_2$ (Eq. A.1 and Eq. A.3). However, we do not account for chemical production in the source term nor deposition in the sink term. The sink of each ffCO$_2$ tags is derived from the negative surface flux $f_{CO_2}^{itag}$, which we define as the product of the negative surface flux of CO$_2$ (f_{CO_2}) at a given time and the ratio of the associated CO$_2$ mixing ratio of the tag ($[CO_2]_{srf}^{itag}$) at the surface and the modeled CO$_2$ mixing ratio $[CO_2]_{srf}$ at the surface; i.e.,

$$f_{CO_2}^{itag} = f_{CO_2} \cdot \left({[CO_2]_{srf}^{itag}} \Big/ {[CO_2]_{srf}} \right) \quad \text{(A.4)}$$

In this manner, the sink of model CO$_2$ can be disaggregated into the sum of the sinks for all tags. This ensures that the relative abundance of the tagged CO$_2$ to the total CO$_2$ is conserved. Other sources of CO$_2$ (chemical oxidation) is treated as part of the "Background+non-ffCO$_2$" in the same manner as the secondary CO within "Background+non-ffCO". Edits to the model include: 1) The CO$_2$ tags are defined in the chemical preprocessor similarly as "CO2_online" (named "CO2_online_anthro", "CO2_online_fire", "CO2_online01", "CO2_online02", …); (2) positive flux (source) files for the tags from specific regions are prepared and defined in the namelist; (4) sinks of all tags are defined using Eq. A.4. The routines, mo_srf_emissions.F90 and chemistry.F90 codes of the CESM chemistry routines are modified for this development. The modified CAM-chem source codes and chemical preprocessor are accessible through Github (See data availability for details).

https://doi.org/10.5194/acp-2020-864
Preprint. Discussion started: 31 August 2020

References

Al-Saadi, Jassim, Gregory Carmichael, James Crawford, Louisa Emmons, Saewung Kim, Chang-Keun Song, Lim-Seok Chang, Gangwoong Lee, Jhoon Kim, Rokjin Park: KORUS-AQ: An International Cooperative Air Quality Field Study in Korea, *the KORUS-AQ white paper* (https://espo.nasa.gov/korus-aq/content/KORUS-AQ_White_Paper), 2014.

Ammoura, L., Xueref-Remy, I., Vogel, F., Gros, V., Baudic, A., Bonsang, B., Delmotte, M., Té, Y., and Chevallier, F.: Exploiting stagnant conditions to derive robust emission ratio estimates for CO_2, CO and volatile organic compounds in Paris, *Atmos. Chem. Phys*., 16, 15653-15664, https://doi.org/10.5194/acp-16-15653-2016, 2016.

Andres, R.J., Boden, T.A., Bréon, F.M., Ciais, P., Davis, S., Erickson, D., Gregg, J.S., Jacobson, A., Marland, G., Miller, J. and Oda, T.: A synthesis of carbon dioxide emissions from fossil-fuel combustion, *Biogeosciences*, 9(5), pp.1845-1871, 2012.

Andres, R.J., Boden, T.A., and Higdon, D.M.: Gridded uncertainty in fossil fuel carbon dioxide emission maps, a CDIAC example, *Atmospheric Chemistry and Physics*, 16, 14979-14995, https://doi.org/10.5194/acp-16-14979-2016, 2016.

Arellano Jr, A.F. and Hess, P.G.: Sensitivity of top-down estimates of CO sources to GCTM transport, *Geophysical research letters*, 33(21), 2006.

Asefi-Najafabady, S., Rayner, P.J., Gurney, K.R., McRobert, A., Song, Y., Coltin, K., Huang, J., Elvidge, C. and Baugh, K.: A multiyear, global gridded fossil fuel CO_2 emission data product: Evaluation and analysis of results, *Journal of Geophysical Research: Atmospheres*, 119(17), pp.10-213, 2014.

Basu, S., Miller, J.B. and Lehman, S.: Separation of biospheric and fossil fuel fluxes of CO_2 by atmospheric inversion of CO_2 and $^{14}CO_2$ measurements: Observation System Simulations. *Atmospheric Chemistry and Physics*, 16(9), 2016.

Basu, S., Lehman, S.J., Miller, J.B., Andrews, A.E., Sweeney, C., Gurney, K.R., Xu, X., Southon, J. and Tans, P.P.: Estimating US fossil fuel CO_2 emissions from measurements of ^{14}C in atmospheric CO_2. *Proceedings of the National Academy of Sciences*, 2020.

Benish, S. E., He, H., Ren, X., Roberts, S. J., Salawitch, R. J., Li, Z., Wang, F., Wang, Y., Zhang, F., Shao, M., Lu, S., and Dickerson, R. R.: Measurement Report: Aircraft Observations of Ozone, Nitrogen Oxides, and Volatile Organic Compounds over Hebei Province, China, Atmos. Chem. Phys. Discuss., https://doi.org/10.5194/acp-2020-194, in review, 2020.

Berhanu, T.A., Szidat, S., Brunner, D., Satar, E., Schanda, R., Nyfeler, P., Battaglia, M., Steinbacher, M., Hammer, S. and Leuenberger, M.: Estimation of the fossil fuel component in atmospheric CO_2 based on radiocarbon measurements at the Beromünster tall tower, Switzerland, *Atmospheric Chemistry and Physics*, 17(17), pp.10753-10766, 2017.

Boesch, H., Baker, D., Connor, B., Crisp, D. and Miller, C.: Global characterization of CO_2 column retrievals from shortwave-infrared satellite observations of the Orbiting Carbon Observatory-2 mission, *Remote Sensing*, 3(2), pp. 270-304, 2011.

Boschetti, F., Thouret, V., Maenhout, G.J., Totsche, K.U., Marshall, J. and Gerbig, C.: Multi-species inversion and IAGOS airborne data for a better constraint of continental-scale fluxes. *Atmospheric Chemistry and Physics*, *18*(13), 9225-9241, 2018.

https://doi.org/10.5194/acp-2020-864
Preprint. Discussion started: 31 August 2020

1169 Bowman, K. W., Liu, J., Bloom, A. A., Parazoo, N. C., Lee, M., Jiang, Z., ... & Wunch, D.: Global
1170 and Brazilian carbon response to El Niño Modoki 2011–2010. Earth and Space Science,
1171 4(10), 637-660, 2017.

1172 Brioude, J., Angevine, W. M., Ahmadov, R., Kim, S.-W., Evan, S., McKeen, S. A., Hsie, E.-Y.,
1173 Frost, G. J., Neuman, J. A., Pollack, I. B., Peischl, J., Ryerson, T. B., Holloway, J., Brown,
1174 S. S., Nowak, J. B., Roberts, J. M., Wofsy, S. C., Santoni, G. W., Oda, T., and Trainer, M.:
1175 Top-down estimate of surface flux in the Los Angeles Basin using a mesoscale inverse
1176 modeling technique: assessing anthropogenic emissions of CO, NOx and CO_2 and their
1177 impacts, *Atmospheric Chemistry and Phys*ics, 13, 3661-3677, https://doi.org/10.5194/acp-
1178 13-3661-2013, 2013.

1179 Chen, S., Xu, L., Zhang, Y., Chen, B., Wang, X., Zhang, X., Zheng, M., Chen, J., Wang, W., Sun,
1180 Y., Fu, P., Wang, Z., and Li, W.: Direct observations of organic aerosols in common
1181 wintertime hazes in North China: insights into direct emissions from Chinese residential
1182 stoves, *Atmospheric Chemistry and Physics*, 17, 1259–1270, https://doi.org/10.5194/acp-
1183 17-1259-2017, 2017.

1184 Cheng, Y., Wang, Y., Zhang, Y., Crawford, J.H., Diskin, G.S., Weinheimer, A.J. and Fried, A.:
1185 Estimator of surface ozone using formaldehyde and carbon monoxide concentrations over
1186 the eastern United States in summer. *Journal of Geophysical Research:*
1187 *Atmospheres*, *123*(14), 7642-7655, 2018.

1188 Chevallier, F., M. Fisher, P. Peylin, S. Serrar, P. Bousquet, F.-M. Bréon, A. Chédin, and P. Ciais:
1189 Inferring CO_2 sources and sinks from satellite observations: method and application to
1190 TOVS data, *Journal of Geophysical Research: Atmospheres*, 110, D24309,
1191 doi:10.1029/2005JD006390, 2005.

1192 Chevallier, F., Ciais, P., Conway, T. J., Aalto, T., Anderson, B. E., Bousquet, P., Brunke, E. G.,
1193 Ciattaglia, L., Esaki, Y., Fröhlich, M., Gomez, A., Gomez-Pelaez, A. J., Haszpra, L.,
1194 Krummel, P. B., Langenfelds, R. L., Leuenberger, M., Machida, T., Maignan, F., Matsueda,
1195 H., Morgui, J. A., Mukai, H., Nakazawa, T., Peylin, P., Ramonet, M., Rivier, L., Sawa, Y.,
1196 Schmidt, M., Steele, L. P., Vay, S. A., Vermeulen, A. T., Wofsy, S., and Worthy, D.: CO2
1197 surface fluxes at grid point scale estimated from a global 21-year reanalysis of atmospheric
1198 measurements, *Journal of Geophysical Research: Atmospheres*, 115, D21307,
1199 doi:10.1029/2010JD013887, 2010.

1200 Chevallier, F.: On the parallelization of atmospheric inversions of CO_2 surface fluxes within a
1201 variational framework, *Geoscientific Model Development*, 6, 783-790,
1202 https://doi.org/10.5194/gmd-6-783-2013, 2013.

1203 Chevallier, F., Palmer, P.I., Feng, L., Boesch, H., O'Dell, C.W. and Bousquet, P.: Toward robust
1204 and consistent regional CO_2 flux estimates from in situ and spaceborne measurements of
1205 atmospheric CO_2, *Geophysical Research Letters*, 41(3), pp.1065-1070, 2014.

1206 Chevallier, F., Description of the CO_2 inversion production chain. CAMS deliverable
1207 CAMS73_2015SC3_D73.1.5.6_201803_CO2 inversion production chain_v1.
1208 http://atmosphere.copernicus.eu/, 2018.

1209 Ciais, P., Paris, J.D., Marland, G., Peylin, P., Piao, S.L., Levin, I., Pregger, T., Scholz, Y., Friedrich,
1210 R., Rivier, L. and Houwelling, S.: The European carbon balance. Part 1: fossil fuel
1211 emissions, *Global Change Biology*, 16(5), pp.1395-1408, 2010.

https://doi.org/10.5194/acp-2020-864
Preprint. Discussion started: 31 August 2020

1212 Ciais, P., Dolman, A.J., Bombelli, A., Duren, R., Peregon, A., Rayner, P.J., Miller, C., Gobron, N.,
1213 Kinderman, G., Marland, G. and Gruber, N.: Current systematic carbon-cycle observations
1214 and the need for implementing a policy-relevant carbon observing system, *Biogeosciences*,
1215 11, pp.3547-3602, 2014.

1216 Ciais, P., Crisp, D., Van Der Gon, H.D., Engelen, R., Janssens-Maenhout, G., Heiman, M., Rayner,
1217 P. and Scholze, M.: Towards a European operational observing system to monitor fossil
1218 CO_2 emissions. Final Report from the expert group, European Commission, 2015.

1219 Crowell, S., Baker, D., Schuh, A., Basu, S., Jacobson, A.R., Chevallier, F., Liu, J., Deng, F., Feng,
1220 L., McKain, K. and Chatterjee, A.: The 2015–2016 carbon cycle as seen from OCO-2 and
1221 the global in situ network. *Atmospheric Chemistry and Physics*, *19*(15), pp.9797-9831,
1222 2019.

1223 Deeter, M. N., Martínez-Alonso, S., Edwards, D. P., Emmons, L. K., Gille, J. C., Worden, H. M.,
1224 Sweeney, C., Pittman, J. V., Daube, B. C., and Wofsy, S. C.: The MOPITT Version 6
1225 product: algorithm enhancements and validation, *Atmospheric Measurement Techniques*,
1226 7, 3623–3632, https://doi.org/10.5194/amt-7-3623-2014, 2014.

1227 Deeter, M.N., Edwards, D.P., Francis, G.L., Gille, J.C., Martínez-Alonso, S., Worden, H.M. and
1228 Sweeney, C.: A climate-scale satellite record for carbon monoxide: the MOPITT Version
1229 7 product, *Atmospheric Measurement Techniques*, 10(7), pp.2533-2555, 2017.

1230 Dlugokencky, E.J., Lang, P.M., Mund, J.W., Crotwell, A.M., Crotwell, M.J., and Thoning, K.W.:
1231 Atmospheric Carbon Dioxide Dry Air Mole Fractions from the NOAA ESRL Carbon
1232 Cycle Cooperative Global Air Sampling Network, 1968-2017, Version: 2018-07-31, Path:
1233 ftp://aftp.cmdl.noaa.gov/data/trace_gases/co2/flask/surface/, 2018.

1234 Dlugokencky, E. J., Lang, P. M., Crotwell, A. M., Masarie, K. A., and Crotwell, M. J.:
1235 Atmospheric Methane Dry Air Mole Frac- tions from the NOAA ESRL Carbon Cycle
1236 Cooperative Global Air Sampling Network, 1983–2014, NOAA ESRL Global Mon-
1237 itoring Division, Boulder, CO, USA, 2015.

1238 Draxler, R.R., Hess, G.D., 1997. Description of the HYSPLIT24 Modeling System. NOAA
1239 Technical Memorandum. ERL ARL-224.

1240 Eldering, A., Wennberg, P.O., Viatte, C., Frankenberg, C., Roehl, C.M. and Wunch, D.: The
1241 Orbiting Carbon Observatory-2: First 18 months of science data products, *Atmospheric*
1242 *Measurement Techniques*, 10(2), pp.549-563, 2017.

1243 Emmons, L. K., Hess, P. G., Lamarque, J. F., & Pfister, G. G.: Tagged ozone mechanism for
1244 MOZART-4, CAM-chem and other chemical transport models. Geoscientific Model
1245 Development, 5(6), 1531, 2012.

1246 Emmons, L.K., Schwantes, R. H., Orlando, J. J., Tyndall, G., Kinnison, D., Lamarque, J. -F.,
1247 Marsh, D., Mills, M., Tilmes, S., Bardeen, C., Buchholz, R. R., Conley, A., Gettelman, A.,
1248 Garcia, R., Simpson, I., Blake, D. R., Meinardi, S., Pétron, G. (2020), The Chemistry
1249 Mechanism in the Community Earth System Model version 2 (CESM2), *J. Advances in*
1250 *Modeling Earth Systems*, 12, https://doi.org/10.1029/2019MS001882.

1251 Enting, I.G.: *Inverse problems in atmospheric constituent transport*. Cambridge University Press,
1252 2002.

https://doi.org/10.5194/acp-2020-864
Preprint. Discussion started: 31 August 2020

1253 Fisher, J. A., Murray, L. T., Jones, D. B. A., and Deutscher, N. M.: Improved method for linear
1254 carbon monoxide simulation and source attribution in atmospheric chemistry models
1255 illustrated using GEOS-Chem v9, *Geoscientific Model Development*, 10, 4129-4144,
1256 https://doi.org/10.5194/gmd-10-4129-2017, 2017.

1257 Gaubert, B., Arellano, A.F., Barré, J., Worden, H.M., Emmons, L.K., Tilmes, S., Buchholz, R.R.,
1258 Vitt, F., Raeder, K., Collins, N. and Anderson, J.L.: Toward a chemical reanalysis in a
1259 coupled chemistry-climate model: An evaluation of MOPITT CO assimilation and its
1260 impact on tropospheric composition, *Journal of Geophysical Research: Atmospheres*,
1261 121(12), pp.7310-7343, 2016.

1262 Gaubert, B., Stephens, B.B., Basu, S., Chevallier, F., Deng, F., Kort, E.A., Patra, P.K., Peters, W.,
1263 Rödenbeck, C., Saeki, T. and Schimel, D.: Global atmospheric CO_2 inverse models
1264 converging on neutral tropical land exchange, but disagreeing on fossil fuel and
1265 atmospheric growth rate, *Biogeosciences*, 16(1), pp.117-134, 2019.

1266 Gaubert, B., Emmons, L. K., Raeder, K., Tilmes, S., Miyazaki, K., Arellano Jr., A. F., Elguindi,
1267 N., Granier, C., Tang, W., Barré, J., Worden, H. M., Buchholz, R. R., Edwards, D. P.,
1268 Franke, P., Anderson, J. L., Saunois, M., Schroeder, J., Woo, J.-H., Simpson, I. J., Blake,
1269 D. R., Meinardi, S., Wennberg, P. O., Crounse, J., Teng, A., Kim, M., Dickerson, R. R.,
1270 He, H., and Ren, X.: Correcting model biases of CO in East Asia: impact on oxidant
1271 distributions during KORUS-AQ, *Atmospheric Chemistry & Physics Discussion*,
1272 https://doi.org/10.5194/acp-2020-599, in review, 2020.

1273 Gelaro, R., McCarty, W., Suárez, M.J., Todling, R., Molod, A., Takacs, L., Randles, C.A.,
1274 Darmenov, A., Bosilovich, M.G., Reichle, R. and Wargan, K.: The modern-era
1275 retrospective analysis for research and applications, version 2 (MERRA-2). *Journal of*
1276 *Climate*, *30*(14), 5419-5454, 2017.

1277 Goo, T.-Y., Y.-S. Oh, V. A. Velazco.: TCCON data from Anmeyondo, South Korea, Release
1278 GGG2014R0. TCCON data archive, hosted by Caltech DATA, California Institute of
1279 Technology, Pasadena, CA, U.S.A.
1280 https://doi.org/10.14291/tccon.ggg2014.anmeyondo01.R0/1149284, 2017.

1281 Graven, H.D., Stephens, B.B., Guilderson, T.P., Campos, T.L., Schimel, D.S., Campbell, J.E. and
1282 Keeling, R.F.: Vertical profiles of biospheric and fossil fuel-derived CO_2 and fossil fuel
1283 CO_2: CO ratios from airborne measurements of $\Delta^{14}C$, CO^2 and CO above Colorado, USA.
1284 *Tellus B: Chemical and Physical Meteorology*, 61(3), pp.536-546, 2009.

1285 Graven, H., Fischer, M.L., Lueker, T., Jeong, S., Guilderson, T.P., Keeling, R.F., Bambha, R.,
1286 Brophy, K., Callahan, W., Cui, X. and Frankenberg, C.: Assessing fossil fuel CO_2
1287 emissions in California using atmospheric observations and models. *Environmental*
1288 *Research Letters*, *13*(6), 2018.

1289 Gurney, K.R., Law, R.M., Denning, A.S., Rayner, P.J., Baker, D., Bousquet, P., Bruhwiler, L.,
1290 Chen, Y.H., Ciais, P., Fan, S. and Fung, I.Y.: TransCom 3 CO_2 inversion intercomparison:
1291 1. Annual mean control results and sensitivity to transport and prior flux information.
1292 *Tellus B: Chemical and Physical Meteorology*, 55(2), pp.555-579, 2003.

1293 Gurney, K.R., Law, R.M., Denning, A.S., Rayner, P.J., Pak, B.C., Baker, D., Bousquet, P.,
1294 Bruhwiler, L., Chen, Y.H., Ciais, P. and Fung, I.Y.: Transcom 3 inversion intercomparison:

https://doi.org/10.5194/acp-2020-864
Preprint. Discussion started: 31 August 2020

Model mean results for the estimation of seasonal carbon sources and sinks, *Global Biogeochemical Cycles*, 18(1), 2004.

Gurney, K.R., Chen, Y.H., Maki, T., Kawa, S.R., Andrews, A. and Zhu, Z.: Sensitivity of atmospheric CO_2 inversions to seasonal and interannual variations in fossil fuel emissions. *Journal of Geophysical Research: Atmospheres*, 110(D10), 2005.

Gurney, K.R., Mendoza, D.L., Zhou, Y., Fischer, M.L., Miller, C.C., Geethakumar, S. and de la Rue du Can, S.: High resolution fossil fuel combustion CO_2 emission fluxes for the United States, *Environmental Science & Technology*, 43(14), pp.5535-5541, 2009.

Halliday, H.S., DiGangi, J.P., Choi, Y., Diskin, G.S., Pusede, S.E., Rana, M., Nowak, J.B., Knote, C., Ren, X., He, H. and Dickerson, R.R.: Using Short-Term CO/CO_2 Ratios to Assess Air Mass Differences Over the Korean Peninsula During KORUS-AQ. *Journal of Geophysical Research: Atmospheres*, 124(20), pp.10951-10972, 2019.

Hedelius, J.K., Liu, J., Oda, T., Maksyutov, S., Roehl, C.M., Iraci, L.T., Podolske, J.R., Hillyard, P.W., Liang, J., Gurney, K.R. and Wunch, D.: Southern California megacity CO_2, CH_4, and CO flux estimates using ground-and space-based remote sensing and a Lagrangian model. *Atmospheric Chemistry and Physics*, *18*(22), pp.16271-16291, 2018.

Hogue, S., Marland, E., Andres, R.J., Marland, G. and Woodard, D.: Uncertainty in gridded CO_2 emissions estimates, *Earth's Future*, 4(5), pp.225-239, 2016.

Houweling, S., Baker, D., Basu, S., Boesch, H., Butz, A., Chevallier, F., Deng, F., Dlugokencky, E.J., Feng, L., Ganshin, A. and Hasekamp, O.: An intercomparison of inverse models for estimating sources and sinks of CO_2 using GOSAT measurements. *Journal of Geophysical Research: Atmospheres*, *120*(10), 5253-5266, 2015.

Hungershoefer, K., Breon, F.-M., Peylin, P., Chevallier, F., Rayner, P., Klonecki, A., Houweling, S., and Marshall, J.: Evaluation of various observing systems for the global monitoring of CO_2 surface fluxes, *Atmos. Chem. Phys*., 10, 10503–10520, doi:10.5194/acp-10-10503-2010, 2010.

Jacob, D. J., et al.: The Tranport and Chemical Evolution over the Pacific (TRACE-P) mission: Design, execution and overview of results, J. Geophys. Res., 108(D20), 9000, doi:10.1029/2002JD003276, 2003.

Jacobson, A. R., Mikaloff Fletcher, S. E., Gruber, N., Sarmiento, J. L., and Gloor, M.: A joint atmosphere–ocean inversion for surface fluxes of carbon dioxide: 1. Methods and global-scale fluxes, Global Biogeochem. Cy., 21, B1019, doi:10.1029/2005GB002556, 2007.

Janssens-Maenhout, G., Crippa, M., Guizzardi, D., Dentener, F., Muntean, M., Pouliot, G., Keating, T., Zhang, Q., Kurokawa, J., Wankmüller, R. and Denier van der Gon, H.: HTAP_v2. 2: a mosaic of regional and global emission grid maps for 2008 and 2010 to study hemispheric transport of air pollution, *Atmospheric Chemistry and Physics*, 15(19), pp.11411-11432, 2015.

Jiang, Z., Jones, D. B. A., Worden, H. M., and Henze, D. K.: Sensitivity of top-down CO source estimates to the modeled vertical structure in atmospheric CO, *Atmospheric Chemistry and Physics*, 15, 1521–1537, https://doi.org/10.5194/acp-15-1521-2015, 2015.

Kaminski, T., Rayner, P.J., Heimann, M. and Enting, I.G.: On aggregation errors in atmospheric

https://doi.org/10.5194/acp-2020-864
Preprint. Discussion started: 31 August 2020

transport inversions. *Journal of Geophysical Research: Atmospheres*, *106*(D5), pp.4703-4715, 2001.

Keppel-Aleks, G., Randerson, J.T., Lindsay, K., Stephens, B.B., Keith Moore, J., Doney, S.C., Thornton, P.E., Mahowald, N.M., Hoffman, F.M., Sweeney, C. and Tans, P.P.: Atmospheric carbon dioxide variability in the Community Earth System Model: Evaluation and transient dynamics during the twentieth and twenty-first centuries, *Journal of Climate*, 26(13), pp.4447-4475, 2013.

Konovalov, I.B., Berezin, E.V., Ciais, P., Broquet, G., Beekmann, M., Hadji-Lazaro, J., Clerbaux, C., Andreae, M.O., Kaiser, J.W. and Schulze, E.D.: Constraining CO_2 emissions from open biomass burning by satellite observations of co-emitted species: a method and its application to wildfires in Siberia, *Atmospheric Chemistry and Physics*, 14, pp.10383-10410, 2014.

Lamarque, J.F., Emmons, L.K., Hess, P.G., Kinnison, D.E., Tilmes, S., Vitt, F., Heald, C.L., Holland, E.A., Lauritzen, P.H., Neu, J. and Orlando, J.J.: CAM-chem: Description and evaluation of interactive atmospheric chemistry in the Community Earth System Model, *Geoscientific Model Development*, 5(2), p.369, 2012.

Lee, H., Dlugokencky, E. J., Turnbull, J. C., Lee, S., Lehman, S. J., Miller, J. B., Petron, G., Lim, J., Lee, G.-W., Lee, S.-S., and Park, Y.-S.: ^{14}C observations of atmospheric CO_2 at Anmyeondo GAW station, Korea: Implications for fossil fuel CO_2 and emission ratios, Atmos. Chem. Phys. Discuss., https://doi.org/10.5194/acp-2020-122, in review, 2020.

Lehner, F., Joos, F., Raible, C. C., Mignot, J., Born, A., Keller, K. M., and Stocker, T. F.: Climate and carbon cycle dynamics in a CESM simulation from 850 to 2100 CE, *Earth System Dynamics*, 6(2), 411-434, 2015.

Levin, I., Kromer, B., Schmidt, M. and Sartorius, H.: A novel approach for independent budgeting of fossil fuel CO_2 over Europe by $^{14}CO_2$ observations, *Geophysical Research Letters*, 30(23), 2003.

Levin, I., Hammer, S., Kromer, B. and Meinhardt, F.: Radiocarbon observations in atmospheric CO_2: determining fossil fuel CO_2 over Europe using Jungfraujoch observations as background, *Science of the Total Environment*, 391(2-3), pp.211-216, 2008.

Levin, I., Naegler, T., Kromer, B., Diehl, M., Francey, R., Gomez-Pelaez, A., Steele, P., Wagenbach, D., Weller, R. and Worthy, D.: Observations and modelling of the global distribution and long-term trend of atmospheric $^{14}CO_2$, *Tellus B: Chemical and Physical Meteorology*, 62(1), pp.26-46, 2010.

Lin, J. C., Gerbig, C., Wofsy, S. C., Andrews, A. E., Daube, B. C., Davis, K. J., and Grainger, C. A.: A near-field tool for sim- ulating the upstream influence of atmospheric observations: The Stochastic Time-Inverted Lagrangian Transport (STILT) model, J. Geophys. Res., 108, 4493, doi:10.1029/2002JD003161, 2003.

Lindenmaier, R., Dubey, M.K., Henderson, B.G., Butterfield, Z.T., Herman, J.R., Rahn, T. and Lee, S.H.: Multiscale observations of CO_2, $^{13}CO_2$, and pollutants at Four Corners for emission verification and attribution, *Proceedings of the National Academy of Sciences*, 111(23), pp.8386-8391, 2014.

Liu, Y., Gruber, N. and Brunner, D.: Spatiotemporal patterns of the fossil-fuel CO_2 signal in central

https://doi.org/10.5194/acp-2020-864
Preprint. Discussion started: 31 August 2020

Europe: results from a high-resolution atmospheric transport model. *Atmospheric Chemistry and Physics*, *17*, 14145-14169, 2017.

Lopez, M., Schmidt, M., Delmotte, M., Colomb, A., Gros, V., Janssen, C., Lehman, S. J., Mondelain, D., Perrussel, O., Ramonet, M., Xueref-Remy, I., and Bousquet, P.: CO, NOx and $^{13}CO_2$ as tracers for fossil fuel CO_2: results from a pilot study in Paris during winter 2010, *Atmospheric Chemistry and Physics*, 13, 7343-7358, https://doi.org/10.5194/acp-13-7343-2013, 2013.

Meinshausen, M., Vogel, E., Nauels, A., Lorbacher, K., Meinshausen, N., Etheridge, D. M., Fraser, P. J., Montzka, S. A., Rayner, P. J., Trudinger, C. M., Krummel, P. B., Beyerle, U., Canadell, J. G., Daniel, J. S., Enting, I. G., Law, R. M., Lunder, C. R., O'Doherty, S., Prinn, R. G., Reimann, S., Rubino, M., Velders, G. J. M., Vollmer, M. K., Wang, R. H. J., and Weiss, R.: Historical greenhouse gas concentrations for climate modelling (CMIP6), *Geoscientific Model Development*, 10, 2057-2116, https://doi.org/10.5194/gmd-10-2057-2017, 2017.

Miller, J.B., Lehman, S.J., Montzka, S.A., Sweeney, C., Miller, B.R., Karion, A., Wolak, C., Dlugokencky, E.J., Southon, J., Turnbull, J.C. and Tans, P.P.: Linking emissions of fossil fuel CO_2 and other anthropogenic trace gases using atmospheric $^{14}CO_2$. *Journal of Geophysical Research: Atmospheres*, 117(D8), 2012.

Moore, J. K., Lindsay, K., Doney, S. C., Long, M. C., and Misumi, K.: Marine ecosystem dynamics and biogeochemical cycling in the Community Earth System Model [CESM1 (BGC)]: Comparison of the 1990s with the 2090s under the RCP4. 5 and RCP8. 5 scenarios, *Journal of Climate*, 26(23), 9291-9312, 2013.

Nassar, R., Jones, D.B., Suntharalingam, P., Chen, J.M., Andres, R.J., Wecht, K.J., Yantosca, R.M., Kulawik, S.S., Bowman, K.W., Worden, J.R. and Machida, T.: Modeling global atmospheric CO_2 with improved emission inventories and CO_2 production from the oxidation of other carbon species, *Geoscientific Model Development*, 3(2), p.689, 2010.

Nassar, R., Napier-Linton, L., Gurney, K.R., Andres, R.J., Oda, T., Vogel, F.R. and Deng, F.: Improving the temporal and spatial distribution of CO_2 emissions from global fossil fuel emission data sets, *Journal of Geophysical Research: Atmospheres*, 118(2), pp.917-933, 2013.

Nathan, B., Lauvaux, T., Turnbull, J. and Gurney, K.: Investigations into the use of multi-species measurements for source apportionment of the Indianapolis fossil fuel CO_2 signal, *Elementa: Science of the Anthropocene*, 6(1), 2018.

National Research Council (NRC): Verifying Greenhouse Gas Emissions: Methods to Support International Climate Agreements, Natl. Acad. Press, Washington, D.C, https://doi.org/10.17226/12883, 2010.

Niu, Z., Zhou, W., Wu, S., Cheng, P., Lu, X., Xiong, X., Du, H., Fu, Y. and Wang, G.: Atmospheric fossil fuel CO_2 traced by $\Delta^{14}C$ in Beijing and Xiamen, China: temporal variations, inland/coastal differences and influencing factors, *Environmental Science & Technology*, 50(11), pp.5474-5480, 2016.

NOAA: Carbon Monoxide (CO) WMO Scale, https://www.esrl.noaa.gov/gmd/ccl/co_scale.html, last access: 25 June, 2020.

https://doi.org/10.5194/acp-2020-864
Preprint. Discussion started: 31 August 2020

1420 O'Dell, C. W., Eldering, A., Wennberg, P. O., Crisp, D., Gunson, M. R., Fisher, B., Frankenberg,
1421 C., Kiel, M., Lindqvist, H., Mandrake, L., Merrelli, A., Natraj, V., Nelson, R. R., Osterman,
1422 G. B., Payne, V. H., Taylor, T. E., Wunch, D., Drouin, B. J., Oyafuso, F., Chang, A.,
1423 McDuffie, J., Smyth, M., Baker, D. F., Basu, S., Chevallier, F., Crowell, S. M. R., Feng,
1424 L., Palmer, P. I., Dubey, M., García, O. E., Griffith, D. W. T., Hase, F., Iraci, L. T., Kivi,
1425 R., Morino, I., Notholt, J., Ohyama, H., Petri, C., Roehl, C. M., Sha, M. K., Strong, K.,
1426 Sussmann, R., Te, Y., Uchino, O., and Velazco, V. A.: Improved retrievals of carbon
1427 dioxide from Orbiting Carbon Observatory-2 with the version 8 ACOS algorithm,
1428 *Atmospheric Measurement Techniques*, 11, 6539-6576, https://doi.org/10.5194/amt-11-
1429 6539-2018, 2018.

1430 Osterman, G. B., Eldering, A., Avis, C., Chafin, B., O'Dell, C. W., Frankenberg, C., Fisher, B. M.,
1431 Mandrake, L., Wunch, D., Granat, R., and Crisp, D.: Orbiting Carbon Observatory-2
1432 (OCO-2) data product user's guide, operational L1 and L2 data versions 8 and 8R, Jet
1433 Propulsion Laboratory, Pasadena, CA, USA, 2016.

1434 Palmer, P.I., Suntharalingam, P., Jones, D., Jacob, D.J., Streets, D.G., Fu, Q., Vay, S.A. and Sachse,
1435 G.W.: Using CO_2: CO correlations to improve inverse analyses of carbon fluxes, *Journal
1436 of Geophysical Research: Atmospheres*, 111(D12), 2006.

1437 Peters, W., Jacobson, A. R., Sweeney, C., Andrews, A. E., Conway, T. J., Masarie, K., Miller, J.
1438 B., Bruhwiler, L., M. P., Pétron, G., Hirsch, A. I., Worthy, D. E. J., van der Werf, G. R.,
1439 Randerson, J. T., Wennberg, P. O., Krol, M. C., and Tans, P. P.: An atmospheric
1440 perspective on North American carbon dioxide exchange: CarbonTracker, *Proceedings of
1441 the National Academy of Sciences*, 104, 18925–18930, doi:10.1073/pnas.0708986104,
1442 2007.

1443 Petzold, A., Thouret, V., Gerbig, C., Zahn, A., Brenninkmei- jer, C.A.M., Gallagher, M., Hermann,
1444 M., Pontaud, M., Ziereis, H., Boulanger, D., Nédélec, P., Smit, H. G. J., Cammas , J.-P.,
1445 Volz-Thomas, A., and the IAGOS Team: Global-Scale Atmosphere Monitoring by In-
1446 Service Aircraft – Current Achievements and Future Prospects of the Euro- pean Research
1447 Infrastructure IAGOS, Tellus B, 67, 28452, https://doi.org/10.3402/tellusb.v67.28452,
1448 2015.

1449 Peylin, P., Houweling, S., Krol, M.C., Karstens, U., Rödenbeck, C., Geels, C., Vermeulen, A.,
1450 Badawy, B., Aulagnier, C., Pregger, T. and Delage, F.: Importance of fossil fuel emission
1451 uncertainties over Europe for CO_2 modeling: model intercomparison, *Atmospheric
1452 Chemistry and Physics*, 11(13), pp.6607-6622, 2011.

1453 Peylin, P., Law, R.M., Gurney, K.R., Chevallier, F., Jacobson, A.R., Maki, T., Niwa, Y., Patra,
1454 P.K., Peters, W., Rayner, P.J. and Rödenbeck, C.: Global atmospheric carbon budget:
1455 results from an ensemble of atmospheric CO_2 inversions, *Biogeosciences*, 10, pp.6699-
1456 6720, 2013.

1457 Quilcaille, Y., Gasser, T., Ciais, P., Lecocq, F., Janssens-Maenhout, G. and Mohr, S.: Uncertainty
1458 in projected climate change arising from uncertain fossil-fuel emission factors,
1459 *Environmental Research Letters*, 13(4), p.044017, 2018.

1460 Rayner, P.J., Raupach, M.R., Paget, M., Peylin, P. and Koffi, E.: A new global gridded data set of
1461 CO_2 emissions from fossil fuel combustion: Methodology and evaluation, *Journal of
1462 Geophysical Research: Atmospheres*, 115(D19), 2010.

https://doi.org/10.5194/acp-2020-864
Preprint. Discussion started: 31 August 2020

1463 Rodgers, C.D.: Inverse methods for atmospheric sounding: theory and practice. World scientific,
1464 https://doi.org/10.1142/3171, 2000.

1465 Saeki, T. and Patra, P.K.: Implications of overestimated anthropogenic CO_2 emissions on East
1466 Asian and global land CO_2 flux inversion, *Geoscience Letters*, 4(1), p.9, 2017.

1467 Sachse, G. W., Collins, J. E. Jr., Hill, G. F., Wade, L. O., Burney, L. G., & Ritter, J. A. (1991).
1468 Airborne tunable diode laser sensor for high-precision concentration and flux
1469 measurements of carbon monoxide and methane. In H. I. Schiff (Ed.), *Measurement of*
1470 *atmospheric gases*, *Proceedings of the Meeting*, (Vol. 1433, p. 157). Bellingham, WA:
1471 Society of Photo-Optical Instrumentation Engineers. https://doi. org/10.1117/12.46162

1472 Sachse, G. W., Hill, G. F., Wade, L. O., & Perry, M. G. (1987). Fast-response, high-precision
1473 carbon monoxide sensor using a tunable diode laser absorption technique. *Journal of*
1474 *Geophysical Research*, *92*(D2), 2071. https://doi.org/10.1029/JD092iD02p02071

1475 Schuh, A. E., Jacobson, A. R., Basu, S., Weir, B., Baker, D., Bowman, K., et al.: Quantifying the
1476 impact of atmospheric transport uncertainty on CO_2 surface flux estimates. *Global*
1477 *Biogeochemical Cycles*, 33, 484- 500. https://doi.org/10.1029/2018GB006086, 2019.

1478 Shiga, Y.P., Michalak, A.M., Gourdji, S.M., Mueller, K.L. and Yadav, V.: Detecting fossil fuel
1479 emissions patterns from subcontinental regions using North American in situ CO_2
1480 measurements, *Geophysical Research Letters*, 41(12), pp.4381-4388, 2014.

1481 Shiomi, K., Kawakami, S., H. Ohyama, K. Arai, H. Okumura, C. Taura, T. Fukamachi, M.
1482 Sakashita.: TCCON data from Saga, Japan, Release GGG2014R0. TCCON data archive,
1483 hosted by CaltechDATA, California Institute of Technology, Pasadena, CA, U.S.A.
1484 https://doi.org/10.14291/tccon.ggg2014.saga01.R0/1149283, 2017.

1485 Silva, S.J., Arellano, A.F. and Worden, H.M.: Toward anthropogenic combustion emission
1486 constraints from space-based analysis of urban CO_2/CO sensitivity, *Geophysical Research*
1487 *Letters*, 40(18), pp.4971-4976, 2013.

1488 Simpson, I., et al.: Characterization, Sources and Reactivity of Volatile Organic Compounds
1489 (VOCs) in Seoul and Surrounding Regions during KORUS-AQ, *Elementa*, in review,
1490 2020.

1491 Stephens, B.B., Gurney, K.R., Tans, P.P., Sweeney, C., Peters, W., Bruhwiler, L., Ciais, P.,
1492 Ramonet, M., Bousquet, P., Nakazawa, T. and Aoki, S.: Weak northern and strong tropical
1493 land carbon uptake from vertical profiles of atmospheric CO*2*, *Science*, 316(5832),
1494 pp.1732-1735, 2007.

1495 Stohl, A., et al.: An analytical inversion method for determining regional and global emissions of
1496 greenhouse gases: Sensitivity studies and application to halocarbons, *Atmospheric*
1497 *Chemistry and Physics*, 9, 1597–1620, doi:10.5194/acp-9-1597-2009, 2009.

1498 Suntharalingam, P., Jacob, D.J., Palmer, P.I., Logan, J.A., Yantosca, R.M., Xiao, Y., Evans, M.J.,
1499 Streets, D.G., Vay, S.L. and Sachse, G.W.: Improved quantification of Chinese carbon
1500 fluxes using CO_2/CO correlations in Asian outflow, *Journal of Geophysical Research:*
1501 *Atmospheres*, 109(D18), 2004.

1502 Suntharalingam, P., Randerson, J.T., Krakauer, N., Logan, J.A. and Jacob, D.J.: Influence of
1503 reduced carbon emissions and oxidation on the distribution of atmospheric CO_2:

https://doi.org/10.5194/acp-2020-864
Preprint. Discussion started: 31 August 2020

1504 Implications for inversion analyses, *Global Biogeochemical Cycles*, 19(4), 2005.

1505 Super, I.: *Quantification and attribution of urban fossil fuel emissions through atmospheric*
1506 *measurements* (Doctoral dissertation, Wageningen University), 2018.

1507 Tang, W., Arellano, A. F., DiGangi, J. P., Choi, Y., Diskin, G. S., Agustí-Panareda, A., Parrington,
1508 M., Massart, S., Gaubert, B., Lee, Y., Kim, D., Jung, J., Hong, J., Hong, J.-W., Kanaya,
1509 Y., Lee, M., Stauffer, R. M., Thompson, A. M., Flynn, J. H., and Woo, J.-H.: Evaluating
1510 high-resolution forecasts of atmospheric CO and CO_2 from a global prediction system
1511 during KORUS-AQ field campaign, *Atmospheric Chemistry and Physics*, 18, 11007-
1512 11030, https://doi.org/10.5194/acp-18-11007-2018, 2018.

1513 Tang, W., Emmons, L. K., Arellano, A. F., Gaubert, B., Knote, C., Tilmes, S., Buchholz, R. R.,
1514 Pfister, G. G., Diskin, G. S., Blake, D. R., Blake, N. J., Meinardi, S., DiGangi, J P., Choi,
1515 Y., Woo, J., He, C., Schroeder, J. R., Suh, I., Lee, H., Jo, H., Kanaya, Y.,Jung, J., Lee, Y.,
1516 and Kim, D.: Source contributions to carbon monoxide concentrations during KORUS-AQ
1517 based on CAM-chem model applications, *Journal of Geophysical Research: Atmospheres*,
1518 124, 10.1029/2018JD029151, 2019a.

1519 Tang, W., Arellano, A. F., Gaubert, B., Miyazaki, K., and Worden, H. M.: Satellite Data Reveals
1520 a Common Combustion Emission Pathway for Major Cities in China, *Atmospheric*
1521 *Chemistry and Physics*, 19, 4269-4288, 10.5194/acp-19-4269-2019, 2019b.

1522 Takahashi, T., Sutherland, S.C., Wanninkhof, R., Sweeney, C., Feely, R.A., Chipman, D.W., Hales,
1523 B., Friederich, G., Chavez, F., Sabine, C. and Watson, A.: Climatological mean and decadal
1524 change in surface ocean pCO2, and net sea–air CO_2 flux over the global oceans. *Deep Sea*
1525 *Research Part II: Topical Studies in Oceanography*, 56(8-10), 554-577, 2009.

1526 Tilmes, S., Hodzic, A., Emmons, L. K., Mills, M. J., Gettelman, A., Kinnison, D. E., et al. (2019).
1527 Climate forcing and trends of organic aerosols in the Community Earth System Model
1528 (CESM2). *Journal of Advances in Modeling Earth Systems, 11*. https://
1529 doi.org/10.1029/2019MS001827.

1530 Turnbull, J.C., Miller, J.B., Lehman, S.J., Tans, P.P., Sparks, R.J. and Southon, J.: Comparison of
1531 $^{14}CO_2$, CO, and SF6 as tracers for recently added fossil fuel CO_2 in the atmosphere and
1532 implications for biological CO_2 exchange, *Geophysical Research Letters*, 33(1), 2006.

1533 Turnbull, J., Rayner, P., Miller, J., Naegler, T., Ciais, P. and Cozic, A.: On the use of $^{14}CO_2$ as a
1534 tracer for fossil fuel CO_2: Quantifying uncertainties using an atmospheric transport model.
1535 *Journal of Geophysical Research: Atmospheres*, 114(D22), 2009.

1536 Turnbull, J. C., Tans, P. P., Lehman, S. J., Baker, D., Conway, T. J., Chung, Y. S., Gregg, J.,
1537 Miller, J. B., Southon, J. R., and Zhou, L. X.: Atmospheric observations of carbon
1538 monoxide and fossil fuel CO_2 emissions from East Asia, *Journal of Geophysical Research:*
1539 *Atmospheres*, 116, D24306, https://doi.org/10.1029/2011JD016691, 2011.

1540 Turnbull, J.C., Sweeney, C., Karion, A., Newberger, T., Lehman, S.J., Tans, P.P., Davis, K.J.,
1541 Lauvaux, T., Miles, N.L., Richardson, S.J. and Cambaliza, M.O.: Toward quantification
1542 and source sector identification of fossil fuel CO_2 emissions from an urban area: Results
1543 from the INFLUX experiment, *Journal of Geophysical Research: Atmospheres*, 120(1),
1544 pp.292-312, 2015.

1545 van der Laan-Luijkx, I. T., van der Velde, I. R., van der Veen, E., Tsuruta, A., Stanislawska, K.,

https://doi.org/10.5194/acp-2020-864
Preprint. Discussion started: 31 August 2020

1546 Babenhauserheide, A., Zhang, H. F., Liu, Y., He, W., Chen, H., Masarie, K. A., Krol, M.
1547 C., and Peters, W.: The CarbonTracker Data Assimilation Shell (CTDAS) v1.0:
1548 implementation and global carbon balance 2001–2015, *Geoscience Model Development*,
1549 10, 2785-2800, https://doi.org/10.5194/gmd-10-2785-2017, 2017.

1550 Vardag, S.N., Gerbig, C., Janssens-Maenhout, G. and Levin, I.: Estimation of continuous
1551 anthropogenic CO_2: model-based evaluation of CO_2, CO, delta^{13}C (CO_2) and delta ^{14}C
1552 (CO_2) tracer methods. *Atmospheric Chemistry and Physics*, *15*(22), 12705-12729, 2015.

1553 Vay, S.A., Choi, Y., Vadrevu, K.P., Blake, D.R., Tyler, S.C., Wisthaler, A., Hecobian, A., Kondo,
1554 Y., Diskin, G.S., Sachse, G.W. and Woo, J.H.: Patterns of CO_2 and radiocarbon across high
1555 northern latitudes during International Polar Year 2008, *Journal of Geophysical Research:*
1556 *Atmospheres*, 116(D14), 2011.

1557 Vogel, F., Hamme, S., Steinhof, A., Kromer, B. and Levin, I.: Implication of weekly and diurnal
1558 ^{14}C calibration on hourly estimates of CO-based fossil fuel CO_2 at a moderately polluted
1559 site in southwestern Germany, *Tellus B: Chemical and Physical Meteorology*, 62(5),
1560 pp.512-520, 2010.

1561 Wang, J.S., Oda, T., Kawa, S.R., Strode, S.A., Baker, D.F., Ott, L.E. and Pawson, S.: The impacts
1562 of fossil fuel emission uncertainties and accounting for 3-D chemical CO_2 production on
1563 inverse natural carbon flux estimates from satellite and in situ data. *Environmental*
1564 *Research Letters*, 2020.

1565 Wang, Y., Munger, J. W., Xu, S., McElroy, M. B., Hao, J., Nielsen, C. P., and Ma, H.: CO_2 and
1566 its correlation with CO at a rural site near Beijing: implications for combustion efficiency
1567 in China, *Atmospheric Chemistry and Physics*, 10, 8881–8897,
1568 https://doi.org/10.5194/acp-10-8881-2010, 2010.

1569 Wang, Y., Broquet, G., Ciais, P., Chevallier, F., Vogel, F., Kadygrov, N., Wu, L., Yin, Y., Wang,
1570 R. and Tao, S.: Estimation of observation errors for large-scale atmospheric inversion of
1571 CO_2 emissions from fossil fuel combustion. *Tellus B: Chemical and Physical Meteorology*,
1572 69(1), p.1325723, 2017.

1573 Wang, Y., Broquet, G., Ciais, P., Chevallier, F., Vogel, F., Wu, L., Yin, Y., Wang, R. and Tao, S.,
1574 2018. Potential of European $^{14}CO_2$ observation network to estimate the fossil fuel CO_2
1575 emissions via atmospheric inversions. *Atmospheric Chemistry and Physics*, *18*(6), 4229-
1576 4250, 2018.

1577 Wiedinmyer, C., Akagi, S.K., Yokelson, R.J., Emmons, L.K., Al-Saadi, J.A., Orlando, J.J. and
1578 Soja, A.J.: The Fire INventory from NCAR (FINN): A high resolution global model to
1579 estimate the emissions from open burning. *Geoscientific Model Development*, *4*(3), 625,
1580 2011.

1581 Worden, H. M., Deeter, M. N., Edwards, D. P., Gille, J. C., Drummond, J. R., and Nédélec, P.:
1582 Observations of near-surface carbon monoxide from space using MOPITT multispectral
1583 retrievals, *Journal of Geophysical Research: Atmospheres*, 115(D18), 2010.

1584 Wu, K., Lauvaux, T., Davis, K.J., Deng, A., Coto, I.L., Gurney, K.R. and Patarasuk, R.: Joint
1585 inverse estimation of fossil fuel and biogenic CO_2 fluxes in an urban environment: An
1586 observing system simulation experiment to assess the impact of multiple
1587 uncertainties. *Elem Sci Anth*, *6*(1), 2018.

https://doi.org/10.5194/acp-2020-864
Preprint. Discussion started: 31 August 2020

Atmospheric Chemistry and Physics Discussions

1588 Wunch, D., Toon, G. C., Blavier, J. F. L., Washenfelder, R. A., Notholt, J., Connor, B. J., Griffith,
1589 D. W., Sherlock, V., and Wennberg, P. O.: The total carbon column observing network,
1590 *Philosophical Transactions of the Royal Society A*, 369, 2087–2112, 2011.

1591 Wunch, D., Toon, G. C., Sherlock, V., Deutscher, N. M., Liu, C., Feist, D. G., and Wennberg, P.
1592 O.: The total carbon column observing network's GGG2014 data version, Carbon Dioxide
1593 Information Analysis Center, Oak Ridge National Laboratory, Oak Ridge, Tennessee, USA,
1594 available at: doi, 10, 2015.

1595 Wunch, D., Wennberg, P. O., Osterman, G., Fisher, B., Naylor, B., Roehl, C. M., O'Dell, C.,
1596 Mandrake, L., Viatte, C., Kiel, M., Griffith, D. W. T., Deutscher, N. M., Velazco, V. A.,
1597 Notholt, J., Warneke, T., Petri, C., De Maziere, M., Sha, M. K., Sussmann, R., Rettinger,
1598 M., Pollard, D., Robinson, J., Morino, I., Uchino, O., Hase, F., Blumenstock, T., Feist, D.
1599 G., Arnold, S. G., Strong, K., Mendonca, J., Kivi, R., Heikkinen, P., Iraci, L., Podolske, J.,
1600 Hillyard, P. W., Kawakami, S., Dubey, M. K., Parker, H. A., Sepulveda, E., García, O. E.,
1601 Te, Y., Jeseck, P., Gunson, M. R., Crisp, D., and Eldering, A.: Comparisons of the Orbiting
1602 Carbon Observatory-2 (OCO-2) XCO_2 measurements with TCCON, *Atmospheric*
1603 *Measurement Techniques*, 10, 2209–2238, https://doi.org/10.5194/amt-10-2209-2017,
1604 2017.

1605 Xia, L., Zhang, G., Liu, L., Li, B., Zhan, M., Kong, P. and Wang, H.: Atmospheric CO_2 and CO
1606 at Jingdezhen station in central China: Understanding the regional transport and
1607 combustion efficiency. *Atmospheric Environment*, *222*, 117104, 2020.

1608 Yin, Y., Bowman, K., Bloom, A.A. and Worden, J.: Detection of fossil fuel emission trends in the
1609 presence of natural carbon cycle variability. *Environmental Research Letters*, *14*(8), 2019.

1610 Yokelson, R.J., Andreae, M.O. and Akagi, S.K.: Pitfalls with the use of enhancement ratios or
1611 normalized excess mixing ratios measured in plumes to characterize pollution sources and
1612 aging. *Atmospheric Measurement Techniques*, 6, p.2155, 2013.

1613 Zhao, C.L. and P.P. Tans: Estimating uncertainty of the WMO mole fraction scale for carbon
1614 dioxide in air, *Journal of Geophysical Research-Atmospheres,* 111(D8),
1615 doi:10.1029/2005JD006003, 2006.

1616 Zheng, B., F. Chevallier, P. Ciais, Y. Yin, M. N. Deeter, H. M. Worden, Y. Wang, Q. Zhang, and
1617 K. He.: Rapid decline in carbon monoxide emissions and export from East Asia between
1618 years 2005 and 2016, *Environmental Research Letters*, 13(4), 044007, doi:10.1088/1748-
1619 9326/aab2b3, 2018.

https://doi.org/10.5194/acp-2020-864
Preprint. Discussion started: 31 August 2020

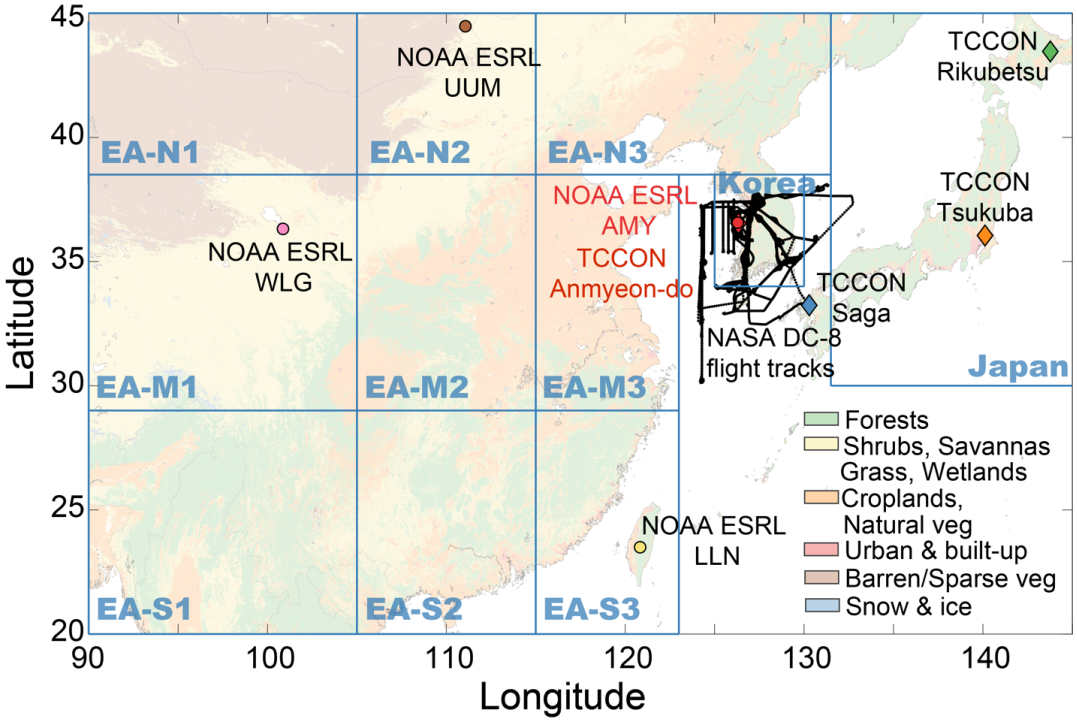

Figure 1. Map of the study domain including: land cover (colored map), definition of tag (basis) regions (blue rectangles), location of four East Asia sites from the NOAA ESRL Carbon Cycle Cooperative Global Air Sampling Network (colored dots), location of East Asia TCCON sites (colored rhombus), and the DC-8 aircraft flight tracks during KORUS-AQ (black lines).

https://doi.org/10.5194/acp-2020-864
Preprint. Discussion started: 31 August 2020

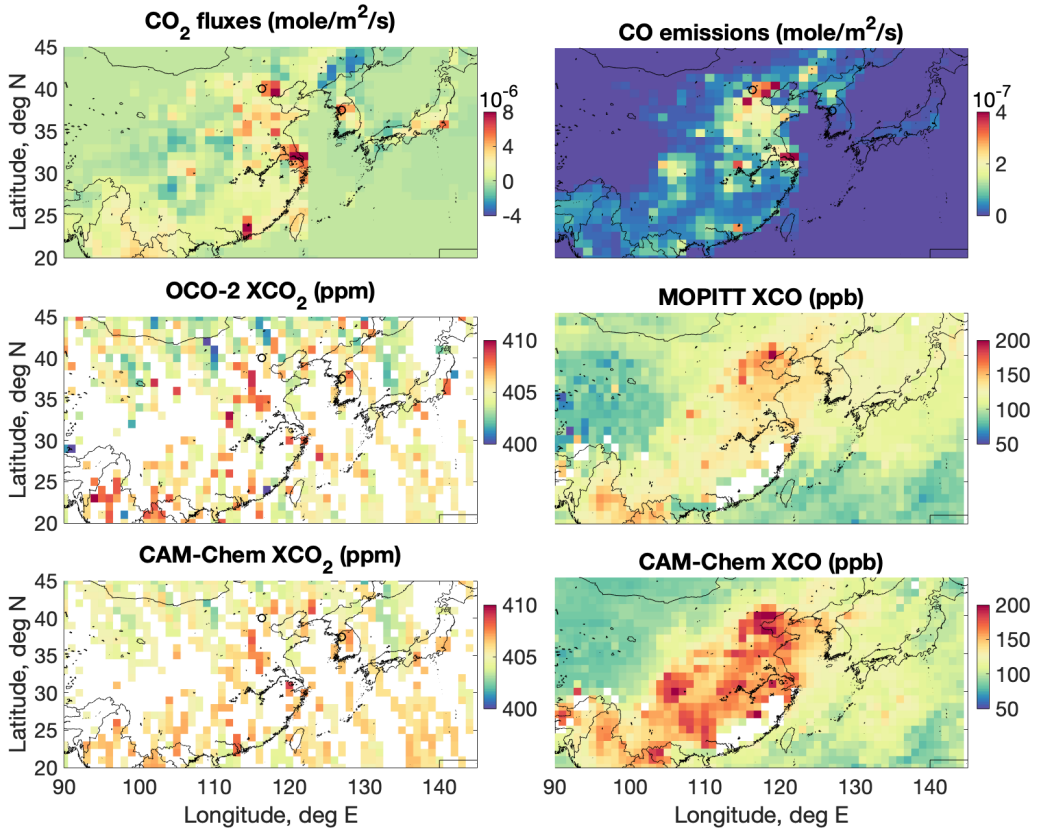

Figure 2. Spatial distribution of *a priori* mean CO_2 fluxes from CT3h (top left), CAM-Chem CO emissions (top, right), OCO-2 XCO_2 (middle left) and MOPITT XCO composites (middle right) for the entire KORUS-AQ campaign period. Also shown is the spatial distribution of CAM-Chem XCO_2 (bottom left) and XCO (bottom right) model equivalents. See Figure S5 for sub-monthly comparisons.

https://doi.org/10.5194/acp-2020-864
Preprint. Discussion started: 31 August 2020

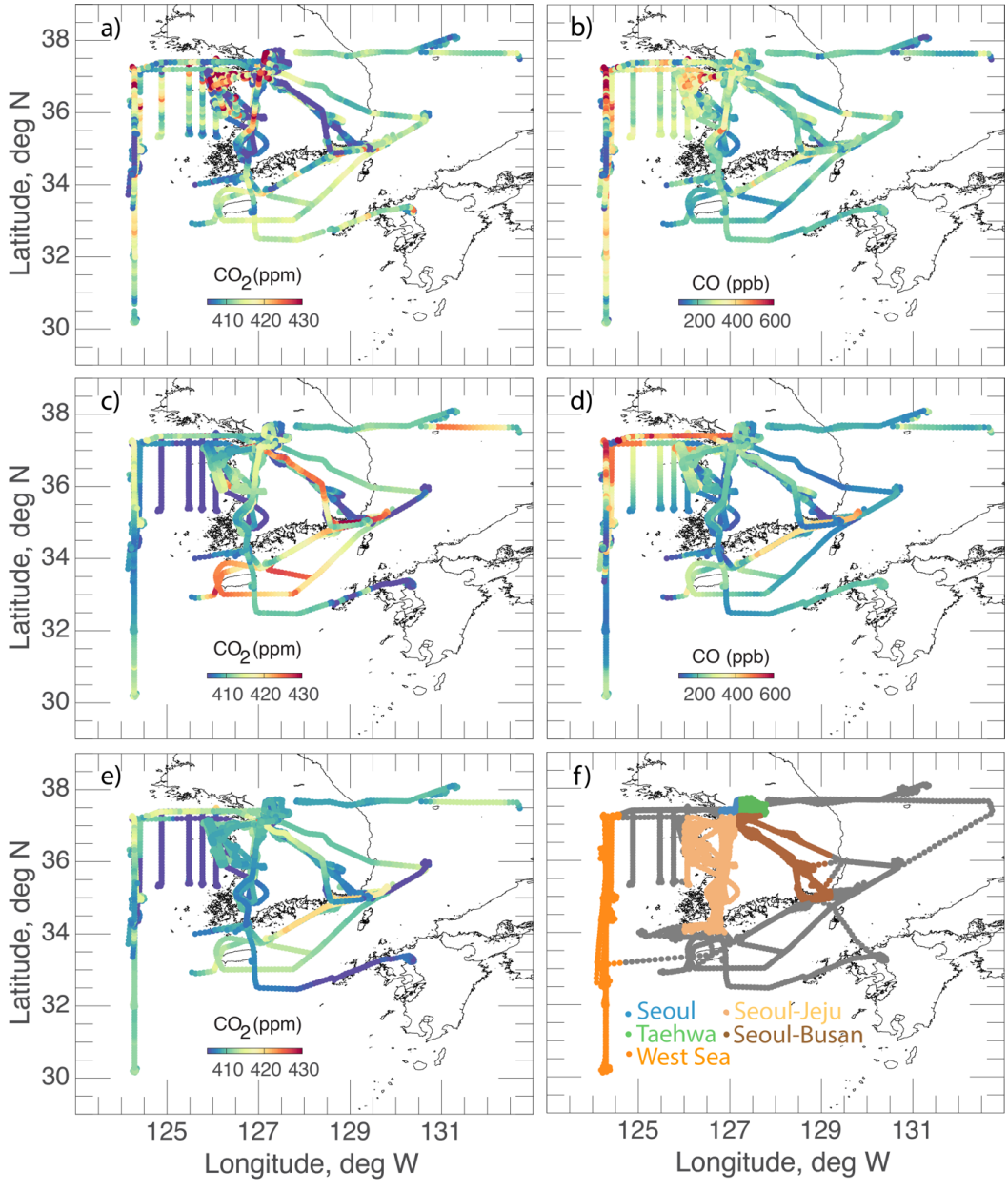

Figure 3. Campaign composite of KORUS-AQ DC-8 flight CO_2 (a) and CO (b) data, model equivalent CO_2 from CAM-Chem (c) and CO (d), and CO_2 from Carbon Tracker (CT2017) CO_2. Panel f) shows the flight tracks for the flight groupings in this study.

https://doi.org/10.5194/acp-2020-864
Preprint. Discussion started: 31 August 2020

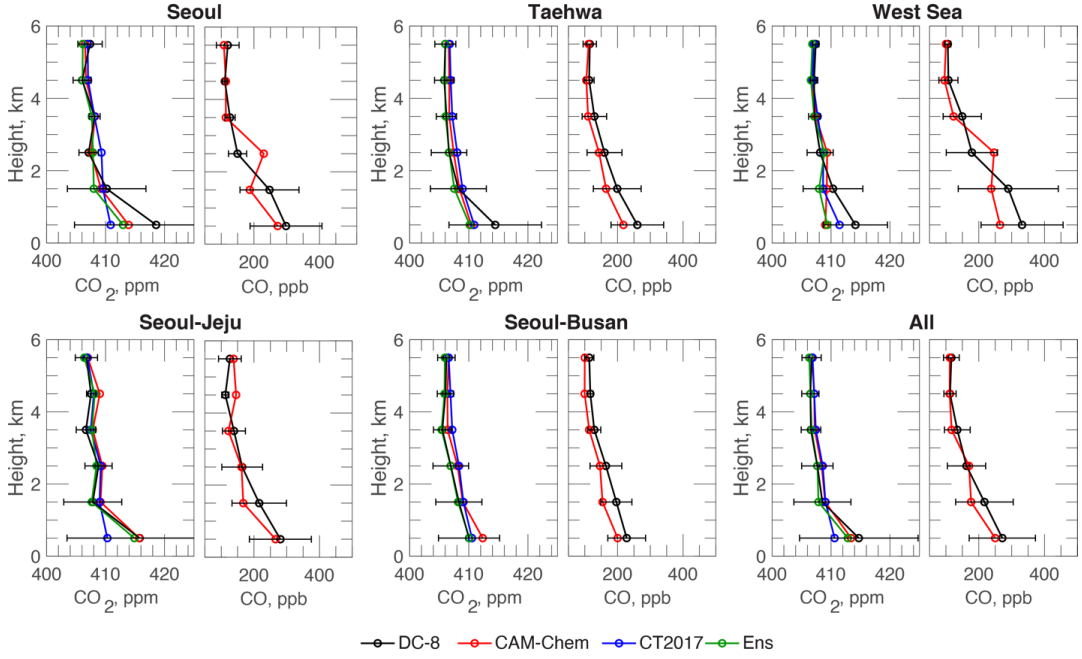

Figure 4. Mean vertical profiles of CO_2 (ppm) and CO (ppb) averaged across the KORUS-AQ campaign period by flight groups (see Figure 3f for the location of these groups). DC-8 data CO_2 and CO are shown in black (with error bars corresponding to its standard deviation). Superimposed are model equivalents of CO_2 and CO from CAM-Chem (red), CO_2 from Carbon Tracker (CT2017, blue), and ensemble mean CO_2 from CAM-Chem using CT3h, CAMS, and CTE2018 fluxes (green).

https://doi.org/10.5194/acp-2020-864
Preprint. Discussion started: 31 August 2020

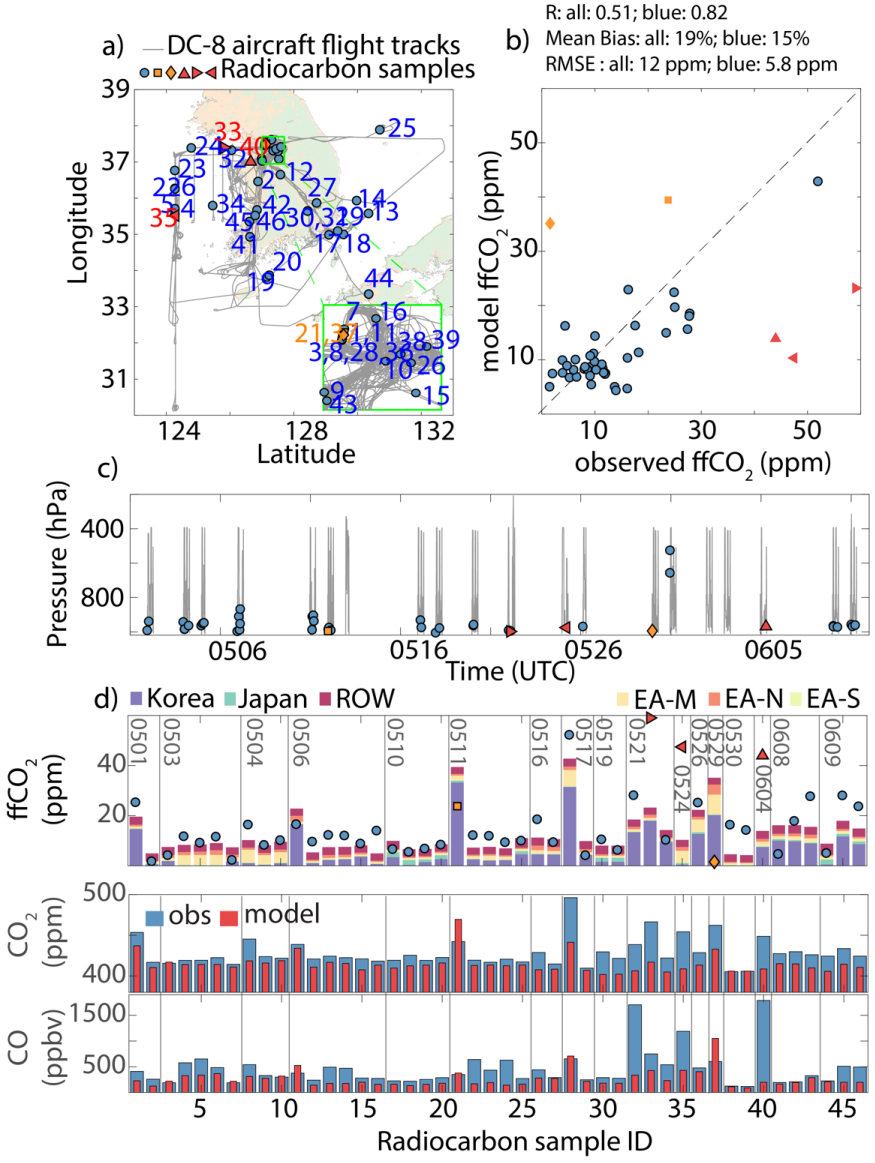

Figure 5. Comparison of $ffCO_2$ with radiocarbon ($^{14}CO_2$) data during KORUS-AQ. The spatial and temporal sampling of $^{14}CO_2$ (colored markers) and CO_2 measurements (gray line) are shown in top left panel (a), (horizontal) and middle panel (c) (vertical and time), respectively. Data points colored in orange and red are considered outliers. The top right panel (b) correspond to a scatterplot between $ffCO_2$ from CAM-chem tags and $ffCO_2$ from $^{14}CO_2$ (overall correlation is indicated for all data points and excluding outliers). Modeled regional contributions to $ffCO_2$ are shown in the bottom panel (d) along with the values of $^{14}CO_2$ samples (ppm), and observed and modeled CO and CO_2 in the bottom panels of d).

https://doi.org/10.5194/acp-2020-864
Preprint. Discussion started: 31 August 2020

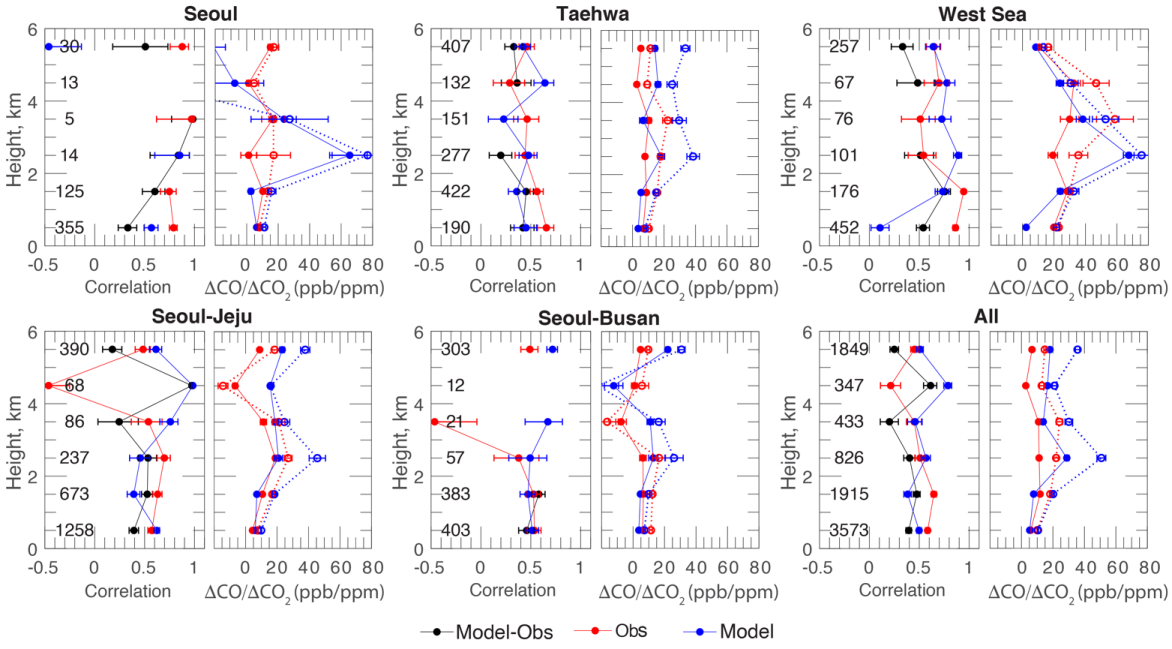

Figure 6. Vertical profiles of mean CO:CO_2 correlations (left panels) from DC-8 (red) and CAM-Chem/CT3h (blue), and the correlation between model CO minus DC-8 CO and model CO_2 minus DC-8 CO_2 (black) arranged by flight groups. Right panels correspond to vertical profiles of derived enhancement ratios (ΔCO: ΔCO_2) from DC-8 (red) and CAM-Chem/CT3h (blue) based on ordinary least squares (OLS) regression. Open circles with dotted lines are enhancement ratios derived using reduced major axis (RMA) regression at $p<0.05$. Number of data points for each vertical layer (1-km) bin is shown in the left panels. The error bar denotes the associated uncertainty of every estimate. Missing values denote non-statistically significant ($p<0.05$) correlations.

https://doi.org/10.5194/acp-2020-864
Preprint. Discussion started: 31 August 2020

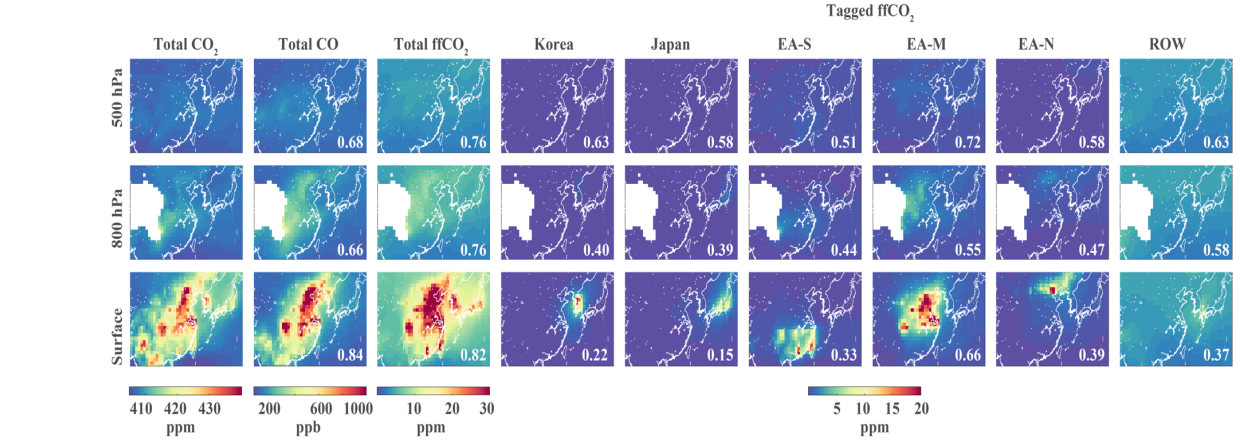

Figure 7. Spatial distribution (averaged across KORUS-AQ) of modeled total CO_2 (ppm) and CO (ppb), modeled $ffCO_2$ and $ffCO_2$ tags at model surface, 800 hPa, and 500 hPa. Pearson (pair-wise) correlation coefficients across the domain relative to total CO_2 are shown in the bottom right of each image.

https://doi.org/10.5194/acp-2020-864
Preprint. Discussion started: 31 August 2020

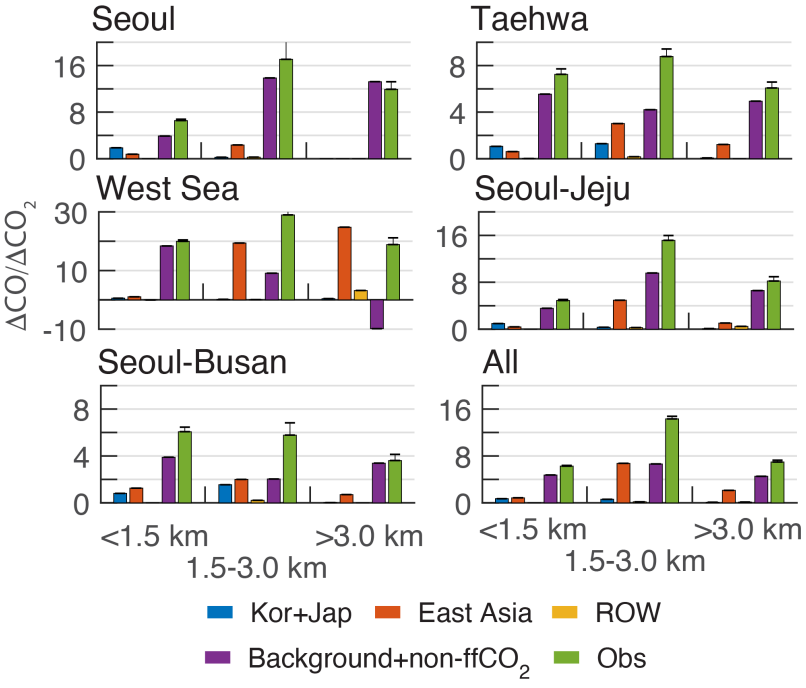

Figure 8. DC-8 ΔCO: ΔCO_2 (green) and associated uncertainty (error bar) derived from all data points within a flight group and vertical layer (0 to 1.5km, 1.5-3.0km and >3.0km). Also shown are contributions of each optimized response functions (based on an inversion using $ffCO_2$ data, see Figure 9) to the overall observed sensitivity.

https://doi.org/10.5194/acp-2020-864
Preprint. Discussion started: 31 August 2020

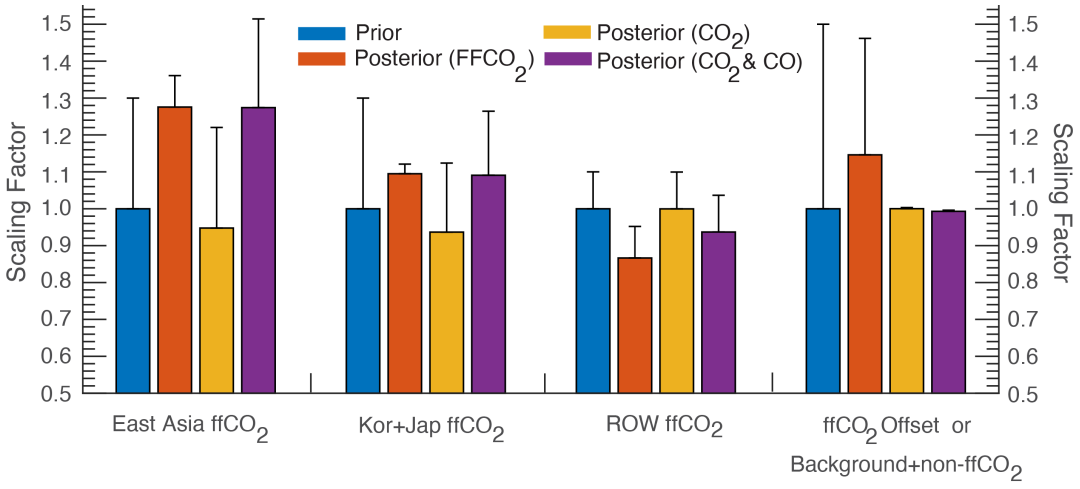

Figure 9. *A priori* (blue) and *a posteriori* estimates of $ffCO_2$ scaling factors (and associated uncertainty shown as an error bar) from a Bayesian synthesis inversion using $ffCO_2$ data derived from $^{14}CO_2$ samples (red) and inversion using DC-8 CO_2 (yellow-orange) and joint inversion using DC-8 CO_2 and CO (magenta). Here, the basis functions are aggregated to include East Asia, Kor+Jap, Rest of the World $ffCO_2$ and "$ffCO_2$ offset" (for $ffCO_2$ inversion) or "Background+non-$ffCO_2$" (for CO_2 or CO_2 and CO inversions).

https://doi.org/10.5194/acp-2020-864
Preprint. Discussion started: 31 August 2020

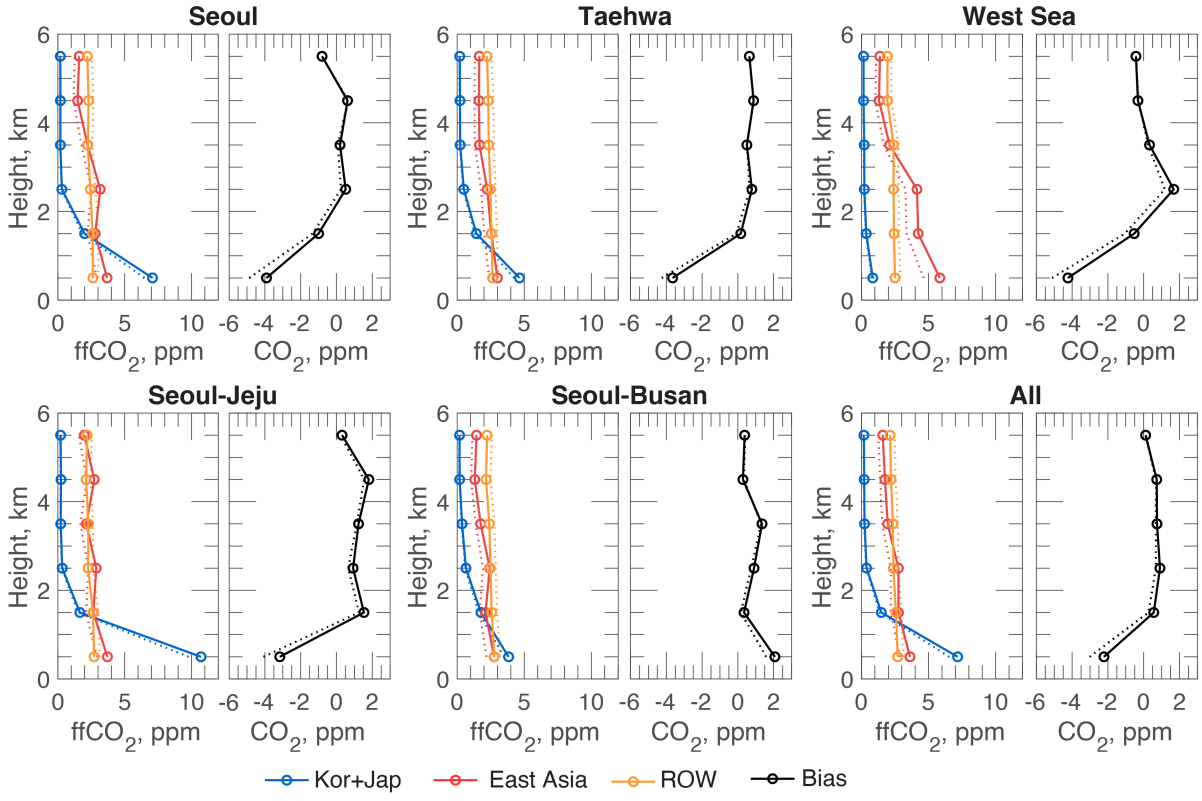

Figure 10. Mean vertical profiles of $ffCO_2$ response functions from Kor+Jap (blue), East Asia (red) and ROW (yellow-orange) for each flight group. Dashed and solid lines correspond to *a priori* and *a posteriori* estimates, respectively. Mean CO_2 bias (model-obs) are shown in the right panels.

https://doi.org/10.5194/acp-2020-864
Preprint. Discussion started: 31 August 2020

Atmospheric Chemistry and Physics Discussions

Table 1. CO_2 fluxes used in this study.

CO_2 fluxes	Spatial Res.	Temporal Res.	Period	Transport Model	Fossil Fuel Priors	Biosphere and Fires Priors	Ocean Priors	Main Reference
CT2017	1° lon 1° lat	3-hourly	2000-2017	TM5	"Miller" (EDGAR scaled to CDIAC) & "ODIAC"	CASA w/ GFED 4.1s GFED_CMS	Jacobson et al. (2007) Takahashi et al (2009)	Peters et al. (2007)[1]

[1]With updates documented at http://carbontracker.noaa.gov.

https://doi.org/10.5194/acp-2020-864
Preprint. Discussion started: 31 August 2020

Atmospheric Chemistry and Physics Discussions

Table 2. Summary statistics of CO and CO_2 NASA DC-8 measurements. npair is the number of data pairs of CO and CO_2. Model equivalents and model evaluation against CO and CO_2 data are also shown. Units are ppm for CO_2 and ppb for CO.

		All	Seoul	Taehwa	West Sea	Seoul Jeju	Seoul Busan
npair		8942	542	1579	1129	2712	1179
Obs Mean	CO_2	410	415	408	411	411	408
	CO	205	266	163	234	223	183
Obs Std	CO_2	7.7	13	5	5	10	4
	CO	101.9	113	73	143	101	64
Obs $R_{CO2,CO}$		0.66	0.79	0.68	0.89	0.62	0.60
Obs $\Delta CO/\Delta CO_2$		13.30	9.13	15.28	28.20	10.37	15.92
Model Mean	CO_2	410	412	408	409	412	410
	CO	188.4	237	143	202	213	155
Model Std	CO_2	7.8	10.5	4.2	3.5	10.1	5.8
	CO	107.1	133	70	119	117	62
Model $R_{CO2,CO}$		0.55	0.59	0.50	0.39	0.67	0.60
Model $\Delta CO/\Delta CO_2$		13.80	12.61	16.56	33.66	11.54	10.68
Bias Model minus Obs	CT3h	-1.0	-3.5	-0.1	-2.2	-1.4	0.8
	CT2017	-1.2	-3.5	-0.4	-1.3	-1.9	0.6
	CO	-24.2	-29.2	-20.4	-32.6	-34.5	-27.9
R Model versus Obs	CT3h	0.39	0.60	0.45	0.40	0.38	0.05
	CT2017	0.37	0.43	0.60	0.51	0.32	0.21
	CO	0.63	0.63	0.64	0.67	0.59	0.72
RMSE	CT3h	7.7	11.0	4.7	5.3	9.3	7.0
	CT2017	6.9	9.8	3.9	4.6	9.0	4.8
	CO	87.6	111.5	64.0	113.6	90.3	55.2
errorR	CT3h	0.40	0.36	0.41	0.57	0.41	0.43